FFI RAPPORT

RANGE LOCALIZATION OF 10-100 KM SHOTS BY MEANS OF AN ENDFIRE ARRAY AND A WAVEGUIDE INVARIANT

SØSTRAND Knut A

FFI/RAPPORT-2002/04849

FFIBM/786/115

Approved
Horten 10 December 2002

Jarl Johnsen
Director of Research

RANGE LOCALIZATION OF 10-100 KM SHOTS BY MEANS OF AN ENDFIRE ARRAY AND A WAVEGUIDE INVARIANT

SØSTRAND Knut A

FFI/RAPPORT-2002/04849

FORSVARETS FORSKNINGSINSTITUTT
Norwegian Defence Research Establishment
P O Box 25, NO-2027 Kjeller, Norway

FORSVARETS FORSKNINGSINSTITUTT (FFI)
Norwegian Defence Research Establishment

P O BOX 25
N0-2027 KJELLER, NORWAY

UNCLASSIFIED

SECURITY CLASSIFICATION OF THIS PAGE
(when data entered)

REPORT DOCUMENTATION PAGE

1) PUBL/REPORT NUMBER	2) SECURITY CLASSIFICATION	3) NUMBER OF PAGES
FFI/RAPPORT-2002/04849	UNCLASSIFIED	43
1a) PROJECT REFERENCE	**2a) DECLASSIFICATION/DOWNGRADING SCHEDULE**	
FFIBM/786/115		

4) TITLE

RANGE LOCALIZATION OF 10-100 KM SHOTS BY MEANS OF AN ENDFIRE ARRAY AND A WAVEGUIDE INVARIANT

5) NAMES OF AUTHOR(S) IN FULL (surname first)

SØSTRAND Knut A

6) DISTRIBUTION STATEMENT

Approved for public release. Distribution unlimited. (Offentlig tilgjengelig)

7) INDEXING TERMS

IN ENGLISH:	IN NORWEGIAN:
a) Underwater acoustics	a) Undervannsakustikk
b) Sound propagation	b) Lydtransmisjon
c) Localization	c) Lokalisering
d) Shallow water	d) Gruntvann
e) Antenna arrays	e) Antenner

THESAURUS REFERENCE:

8) ABSTRACT

During a shallow-water acoustic experiment, signals from small explosions were recorded on an endfire horizontal array. The experiment took place in open waters with relatively slow changes of the water depth with range. The array in question (820 m) proved to be too short for measuring group speeds of individual modes, but resolved the phase speeds well. By means of the "β waveguide invariant" relationship between group and phase speed, the ranges of the shots were estimated from the phase speeds and the arrival time differences, and compared to the ranges obtained by navigation. Similarly, β values were estimated for the individual shots and compared to theoretical values computed according to assumptions such as the adiabatic approximation.

9) DATE	AUTHORIZED BY	POSITION
	This page only	
10 December 2002	Jarl Johnsen	Director of Research

CONTENTS

RANGE LOCALIZATION OF 10-100 KM SHOTS BY MEANS OF AN ENDFIRE ARRAY AND A WAVEGUIDE INVARIANT

1 INTRODUCTION

If two phenomena (signals) start out simultaneously from the same position at speeds u_1 and u_2, respectively, they will arrive at range R with time difference

$$T_2 - T_1 = \frac{R}{u_2} - \frac{R}{u_1} \tag{1.1}$$

This can be written

$$R = \frac{T_2 - T_1}{\frac{1}{u_2} - \frac{1}{u_1}} = \frac{T_2 - T_1}{S_g^2 - S_g^1} = \frac{\Delta T}{\Delta S_g} \tag{1.2}$$

In the context of signals in waveguides, u is termed *group speed,* the speed by which a sound signal envelope travels horizontally. u_1 and u_2 may refer to two different normal modes or two different frequencies of the same mode. It is convenient also to operate with group slowness S_g, which is the inverse of group speed u.

Phase speed is the horizontal speed of the zero crossings of the signal. In principle group speed and phase speed can be measured by hydrophones in-line with the propagation direction, such as endfire arrays. Phase speed is easier to measure than group speed, because it requires shorter arrays. The main reason is that the signal envelopes have much lower frequency content than the signals they enclose. In practice, a direct group speed measurement may require an array that is prohibitively long. The approach taken here is to use phase speed measurements for range estimation.

In many situations there is a fixed relationship between group slowness and phase slowness *differences*, a so-called *waveguide invariant*, usually named β

$$\beta = -\frac{S_p^2 - S_p^1}{S_g^2 - S_g^1} = -\frac{\Delta S_p}{\Delta S_g} \tag{1.3}$$

If this relation is known, phase slowness can be used in the range estimation formula

$$R = -\beta \frac{T_2 - T_1}{S_p^2 - S_p^1} = -\beta \frac{\Delta T}{\Delta S_p} \tag{1.4}$$

Using data from an experiment to be described in Chapter 2, it has been possible to check the applicability of Equation (1.4) by measuring both group and phase slowness. Some signal structures are described in Chapter 3. Expressions for determining β theoretically in waveguides with varying water depths are given in Chapter 4. An analogy with the Pekeris waveguide is also discussed. The signal processing appropriate for extracting β is described in Chapter 5, and comparisons between measured and theoretical β values are made. In Chapter 6 actual range estimates by use of Equation (1.4) are found and compared to the true ranges. These estimates are based solely upon beamformer outputs, knowledge of the bottom and top bedrock profiles with range, and a rough indication of the average water sound speed, no other geophysical information.

2 DESCRIPTION OF EXPERIMENT

During an experiment in the Barents Sea in August 1999 (1, 2) a hydrophone array system was deployed roughly 100 nautical miles NE of North Cape. The main purpose was to provide signals for studies of matched field inversion and localization, but with openings for other kinds of signal processing. One such method is treated here.

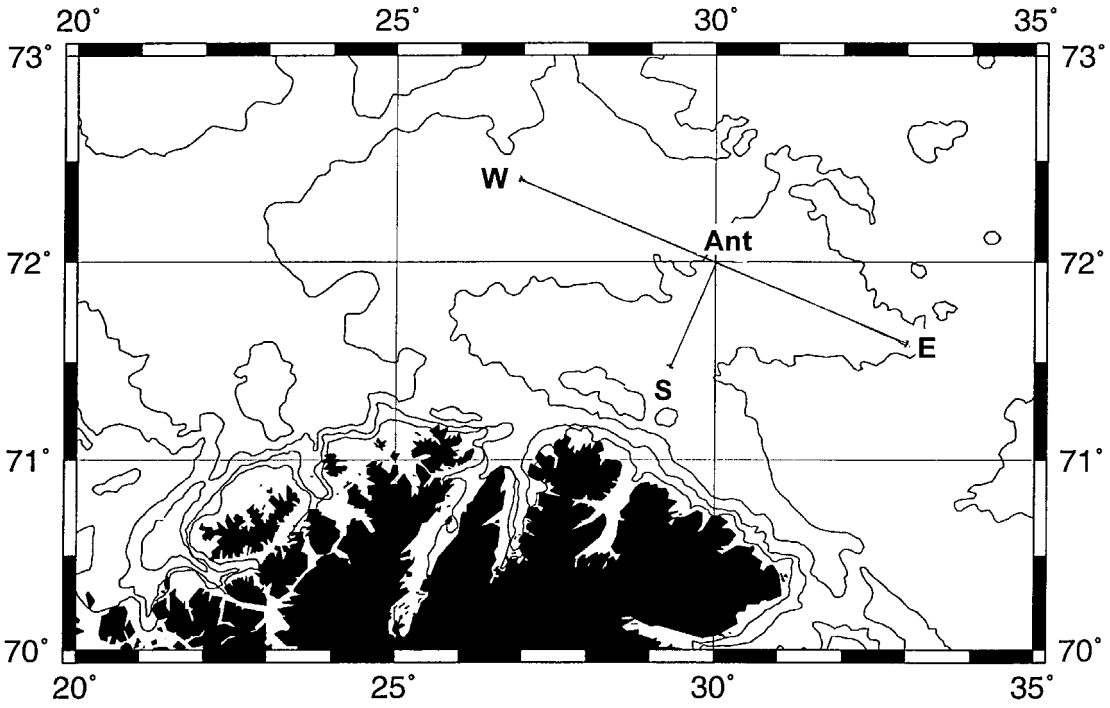

Figure 2.1 Experimental area

The hydrophone array was deployed at the bottom at 72° N and 30° E in 320 m sea depth with longitudinal orientation close to 115°, Figure 2.1. The part of the hydrophone array which is relevant for the present study is shown in Figure 2.2.

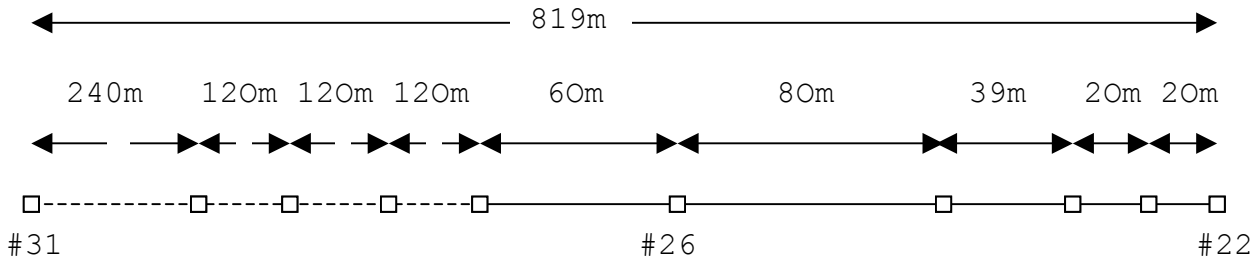

Figure 2.2 Experimental array

Sound sources were SUS charges, dropped along the tracks given in Figure 2.1. Of concern here are only the W and E tracks, both extending more than 100 km from the array. Shallow (18 m), intermediate (90 m) and deep (240 m) SUS charges were used, in total 222 charges for this part of the experiment.

Accurate drop positions and detonation times were logged at the source ship (P-code GPS). The ship was moving at constant speed. Shallow charges had to be dropped by means of a pneumatic launcher. Detonation times were logged using a towed hydrophone. Positions and detonation times had later to be corrected for the local offsets (3). At the receiving site the GPS time code was recorded together with the signals. Thereby very accurate ranges and travel times could be established. Appendix A comments upon this.

Separate runs provided geophysical information along the tracks (seismic reflection profiles and refraction velocity measurements) (4). A sediment layer of varying thickness is overlying the bedrock, as shown in Figure 2.3. Estimated (typical) values for sound speed etc are indicated. Beyond 70 km East of the receiver the sediment layer was too thin to be read off properly. Water depth was taken from echo soundings. Some sound velocity profiles taken during the experiment are shown in Figure 2.4. Notwithstanding some variability, at the outset the area could be characterized as relatively simple and homogeneous acoustically.

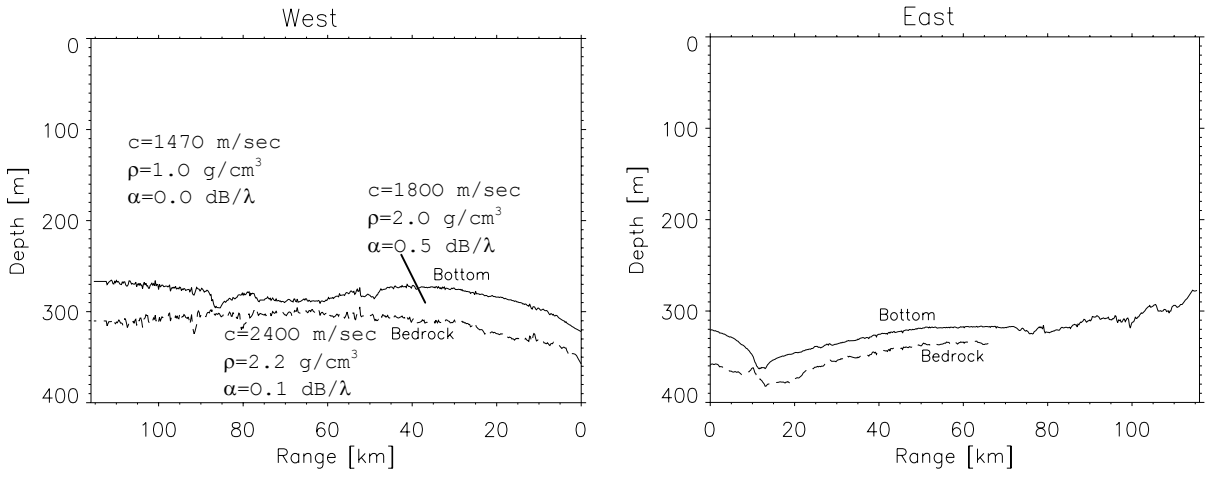

Figure 2.3 Bottom and top bedrock profiles. Geophysical parameters from (4)

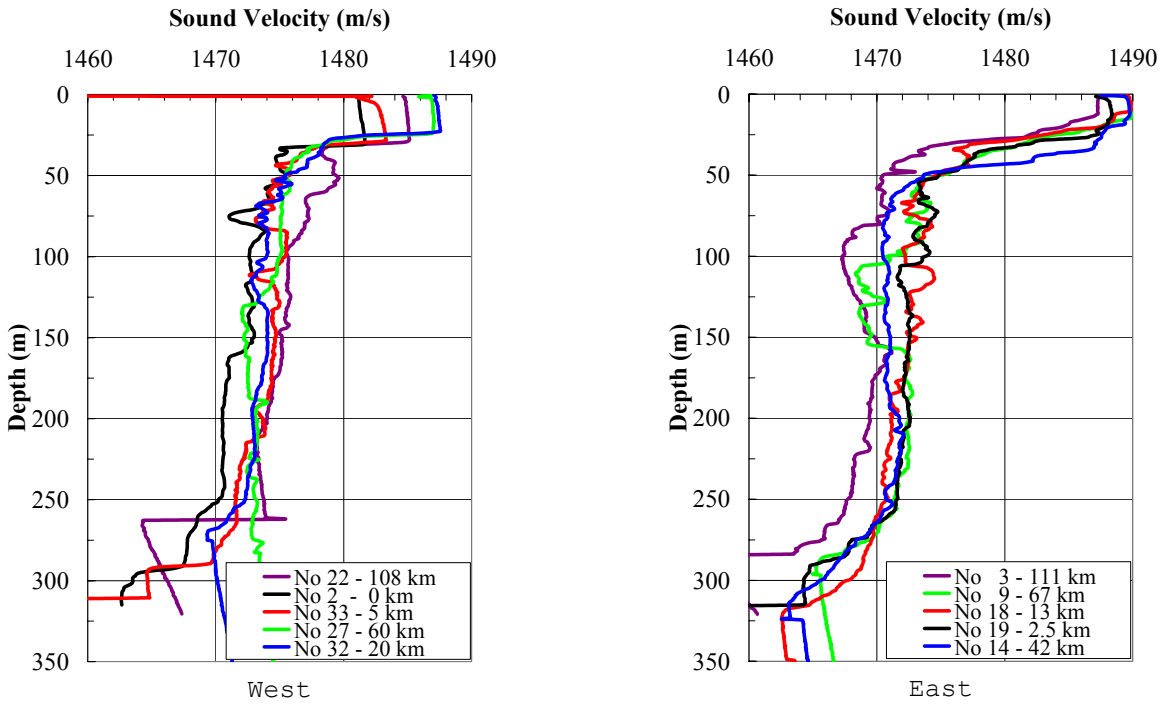

Figure 2.4 Sound velocity profiles

3 SIGNAL STRUCTURES

The received shot signals showed very clear normal mode structures in time/frequency and in angular (vertical) dimensions. Two examples of "Lofargrams" for 18 m shots are shown in Figure 3.1, from the W run at range 28 km and from the E run at range 51 km. In producing these diagrams single-hydrophone signals were passed through a bank of 1/12 octave filters (±3% bandwidth) with 1/48 octave between center frequencies. The patterns show well distinguishable mode delays, with a very weak Mode 1 (top, smallest delay) and strong Modes 2 - 5,6. Weaker modes at higher indices can be seen. The mode identification will be commented upon in Section 4.4. Clear mode patterns can be seen up to about 40 - 50 Hz, where the arrivals become more random.

The modes have in general a single delay maximum at a certain frequency, i e group speed minimum. This is a behavior typical of the Pekeris waveguide. This point is discussed in Section 4.4. The turning points, here recognizable for modes M2 – 4,5, are related to the cut-off frequencies for the different modes. They are different for the two shots. In fact, the cut-off frequencies are determined by the shallowest part of the waveguide between source and receiver. Referring to Figure 2.3, the cut-off frequencies should be expected to remain constant for sources outside 40 km during the W run, and for sources inside 70 km during the E run.

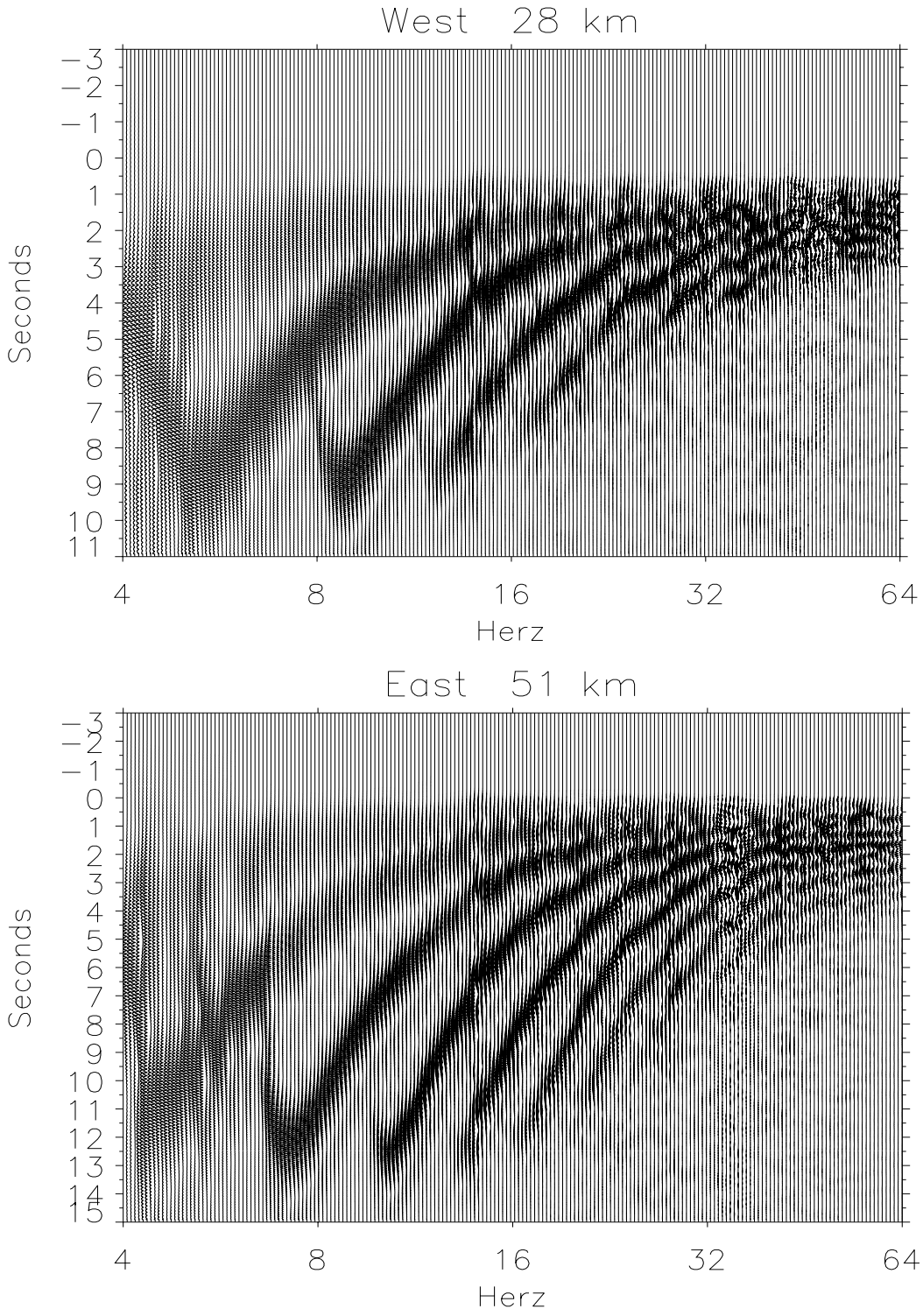

Figure 3.1 Spectrograms or 'Lofargrams' for two sample shots
Frequency resolution = 1/12 octave (±3%)
Each filter output is normalized to max = 1

Taking the signals from any particular 1/12 octave band and using all the hydrophones in the array, the signal set can be beamformed. An unweighted delay-and-sum beamformer was applied, which seemed reasonable when operating with transient signals. After squaring and some smoothing, results for the 51 km E shot are shown in Figure 3.2, at six different frequencies. The main "blobs" are modes, which arrive at different times and vertical angles. Note that the directional scale is not in incidence angle θ itself, but in sin θ. Comparison with Figure 3.1 at frequencies in question will verify the number of modes and their delays. More details about a beamformer operating on transient signals in a dispersive medium are given in Appendix B.

From Figure 3.2 it can be seen that the mode maxima follow straight lines fairly closely. The slope values of the lines are nearly the same for all frequencies. This is a manifestation of a waveguide invariant. The slopes will be different for different shots, becoming steeper with increasing range, making range discrimination possible. *This is the main clue of the study.*

Straight line patterns can be seen up to relatively high frequencies, typically 200 Hz, which is far above where the mode patterns in the time/frequency diagram (Figure 3.1) disappears. This means that invariance is retained, even if individual mode arrivals fluctuate.

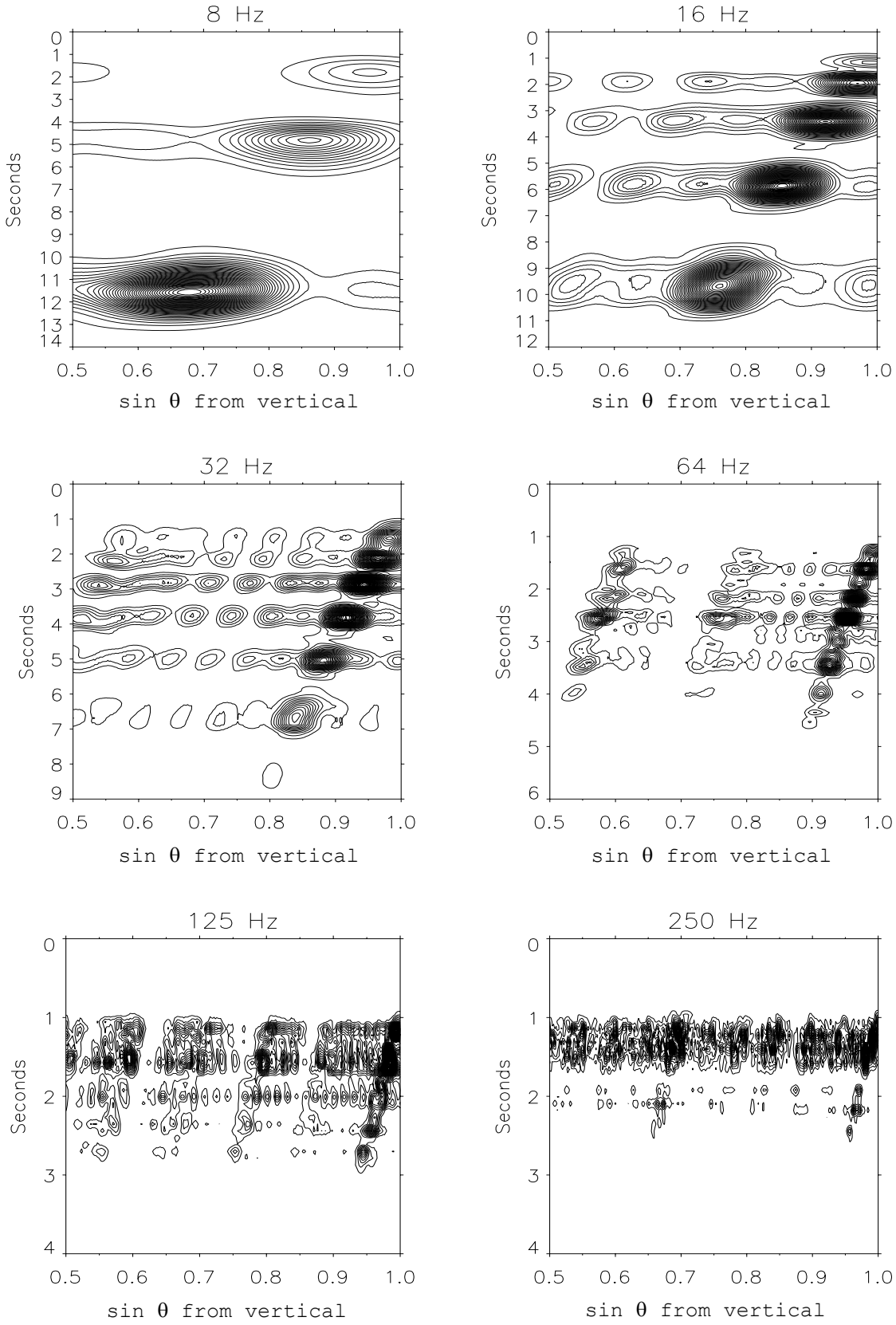

Figure 3.2 Beam versus time diagrams for the Eastern 51 km shot at six frequencies
Filter bandwidths = 1/12 octave
θ = angle of incidence Vertical: θ=0° Endfire: θ=90°

4 THE WAVEGUIDE INVARIANT β

4.1 Constant waveguide

The definition of the waveguide invariant β is in accordance with (5, 6, 7). Slightly rewriting Equation (1.4),

$$\beta = -\frac{S_p^m - S_p^n}{S_g^m - S_g^n} = -\frac{\Delta S_p}{\Delta S_g} \tag{4.1}$$

Here m and n are mode indices or frequency indices (or combinations). Equation (4.1) expresses the relation between phase and group slowness differences in the mode-number/frequency plane.

In a constant waveguide there are no depth or speed changes etc with range, and β will be constant with range for certain mode groups and frequency intervals (6,7). A waveguide with reflecting bottom will have a β different from the β of a surface channel waveguide, for instance.

4.2 Adiabatic waveguide

When the waveguide parameters are slowly changing with range and there is no energy transfer between modes, the waveguide is said to be "adiabatic". Then the invariant β itself will be a function of range according to the expression (5, 7)

$$\beta(r) = -\frac{\Delta S_p(rec)}{\Delta \bar{S}_g(r)} \tag{4.2}$$

Here $S_p(rec)$ is phase slowness at the receiver and $\bar{S}_g(r)$ is average group slowness over the range. Conveniently, this is what the experiment provides, the phase slowness measurement is local at the array, and the group slowness measurement is an average over range. Thus changes in β over range are determined by the change in average group slowness.

4.3 Adiabatic "ideal" waveguide

Assuming that the adiabatic waveguide has constant sound speed but varying water depth with reflecting bottom, and that β(0) = 1 at the receiver site (i e for very short ranges), then β will be a function of range according to the expression (7)

$$\frac{1}{\beta(r)} \approx D^2(rec)\frac{1}{r}\int_0^r \frac{dx}{D^2(x)} \tag{4.3}$$

4.4 The invariant β and a Pekeris waveguide analogy

It was indicated earlier that the present waveguide had some features similar to the Pekeris waveguide. This will now be looked into.

Using the minima of Figure 3.1, related to the cut-off frequencies, which again are determined mainly by water depth and water/bottom sound speeds, rough Pekeris analogues could easily be found. It soon became clear that the sediment sound speed of 1800 m/sec was too low to obtain a fit, and that a speed closer to the nominal bedrock speed of 2400 m/sec had to be used instead. Using 2300 m/sec and the top of bedrock instead of the sea bottom gave good correspondence, shown in Figure 4.1. The resulting parameter values are indicated. That the sediment should be somewhat transparent at these low frequencies seems reasonable. Comparing Figure 4.1 to Figure 3.1 indicates strongly that the mode indices as given in Chapter 3 are correct.

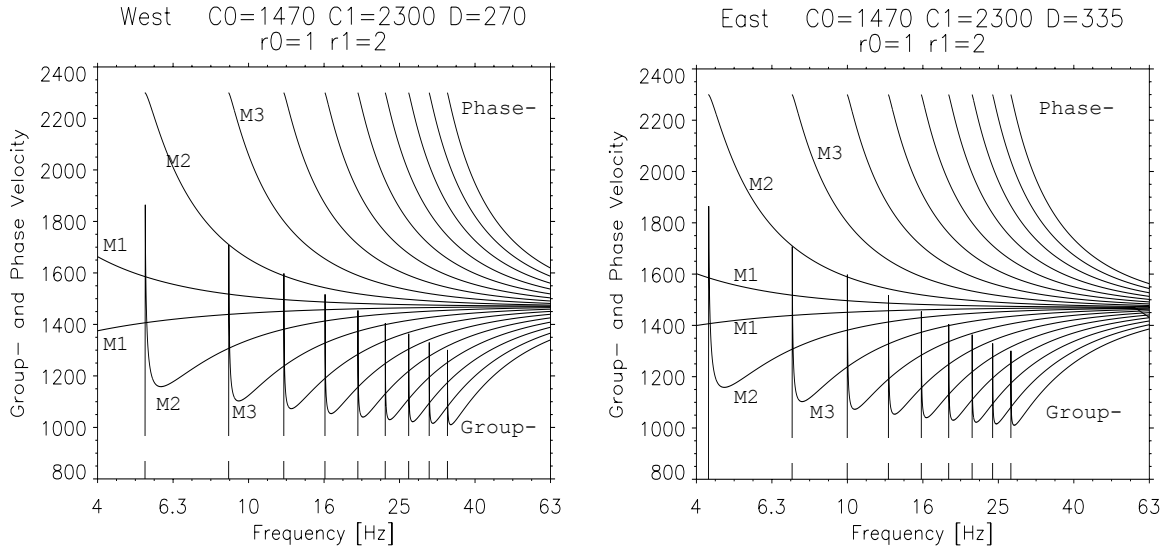

Figure 4.1 Phase speeds and group speeds versus frequency for two Pekeris analogues

These Pekeris waveguide approximations will now be developed further, for demonstrating the point that within some restrictions $\beta \approx 1$. Taking corresponding pairs of phase and group speeds for each frequency and mode and plotting slownesses against each other gives the diagram of Figure 4.2 (left). It turns out that the S_g versus S_p diagrams for the two cases above will look identical. The basis for this is that the group and phase speeds are functions of the dimensionless quantity $D \cdot f/c_0$. The slope (negative) of a curve in Figure 4.2 (left) corresponds to $1/\beta$ (over frequency) for the mode in question. In the diagram are also put straight lines for $\beta = 1.0 \pm 10\%$.

At small phase slowness, especially near the curve minima, there can be a large spread of β values from one mode to the other. However, at higher phase slowness, except for Mode 1 and partly Mode 2, the modes have β in the vicinity of 1.0. Within ±10% this applies above

Sp=0.0006, corresponding to sinθ > 0.88 , i e grazing angles less than 30°. As will be shown later, the most useful frequency interval for range estimation turns out to be 20 – 80 Hz. Figure 4.2 (right) is similar to the earlier diagram, but covers only these frequencies. There is very little β spread between the modes in this frequency interval.

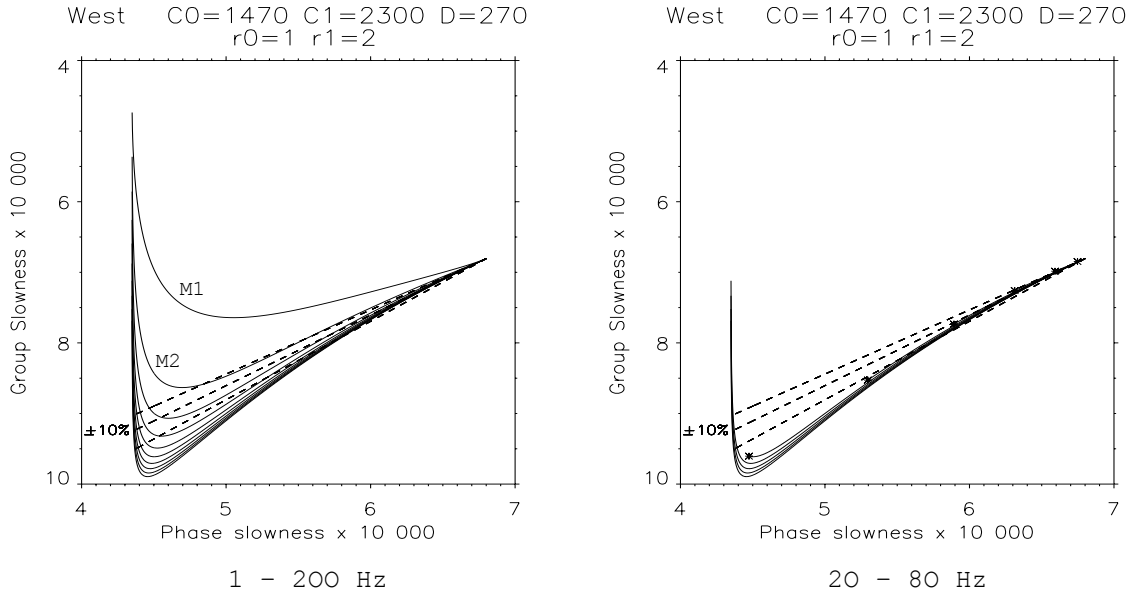

Figure 4.2 Group slowness versus phase slowness for Pekeris analogue
Dotted lines: $\beta = 1.0 \pm 10\%$

The information in Figure 4.2 could also be plotted as curves for individual frequencies. This is not shown here, as such diagrams become rather messy because of the discrete nature of the modes. A recommendation drawn from Figure 4.2 would be to stay well away from the cutoffs for the present application.

The Pekeris analogy was introduced mainly in support of $\beta \approx 1$. No other Pekeris-derived parameters will be used for the final range estimation.

5 MEASUREMENTS OF THE INVARIANT β

5.1 Group versus phase slowness diagram

It will now be shown how diagrams like those in Figure 3.2 can be transformed into group slowness versus phase slowness diagrams simply by changing units along the axes. Then the slope of the pattern will determine 1/β. This is shown in Figure 5.1, which is an enlargement of the 16 Hz diagram of Figure 3.2.

Horizontal axis. The horizontal scale (sin θ) is proportional to phase slowness S_p, because the horizontal phase slowness is

$$S_p = \frac{\sin\theta}{c_0} \tag{5.1}$$

c_0 is the water sound speed at the array. Therefore sinθ=1 corresponds to $S_p=1/c_0$, sinθ=0.5 corresponds to $S_p=1/(2c_0)$ and sinθ=0 would correspond to $S_p=0$. Part of this is written into Figure 5.1. Therefore for phase slowness differences,

$$\Delta S_p = \frac{\Delta\sin\theta}{c_0} \tag{5.2}$$

Vertical axis. In the vertical direction (time dimension) the mode envelopes will show up at their respective delays or travel times. Travel time is proportional to group slowness. Referring to Figure 5.1, t=0 will correspond to $S_g=0$ because zero travel time corresponds to infinite speed. T_0 is the shortest possible travel time, corresponding to horizontal speed c_0. Then $S_g=1/c_0$ at T_0. This is also written into Figure 5.1. The number of S_g units per time unit is therefore $1/(c_0\,T_0)$. Then for group slowness,

$$S_g = \frac{t}{c_0 T_0} \tag{5.3}$$

For the differences,

$$\Delta S_g = \frac{\Delta T}{c_0 T_0} \tag{5.4}$$

Travel time T_0 for all the shots was measured during the experiment. It was actually measured from the first arrivals of the high frequency part of the shot. All information needed for measuring β is now available through measurement of the slope.

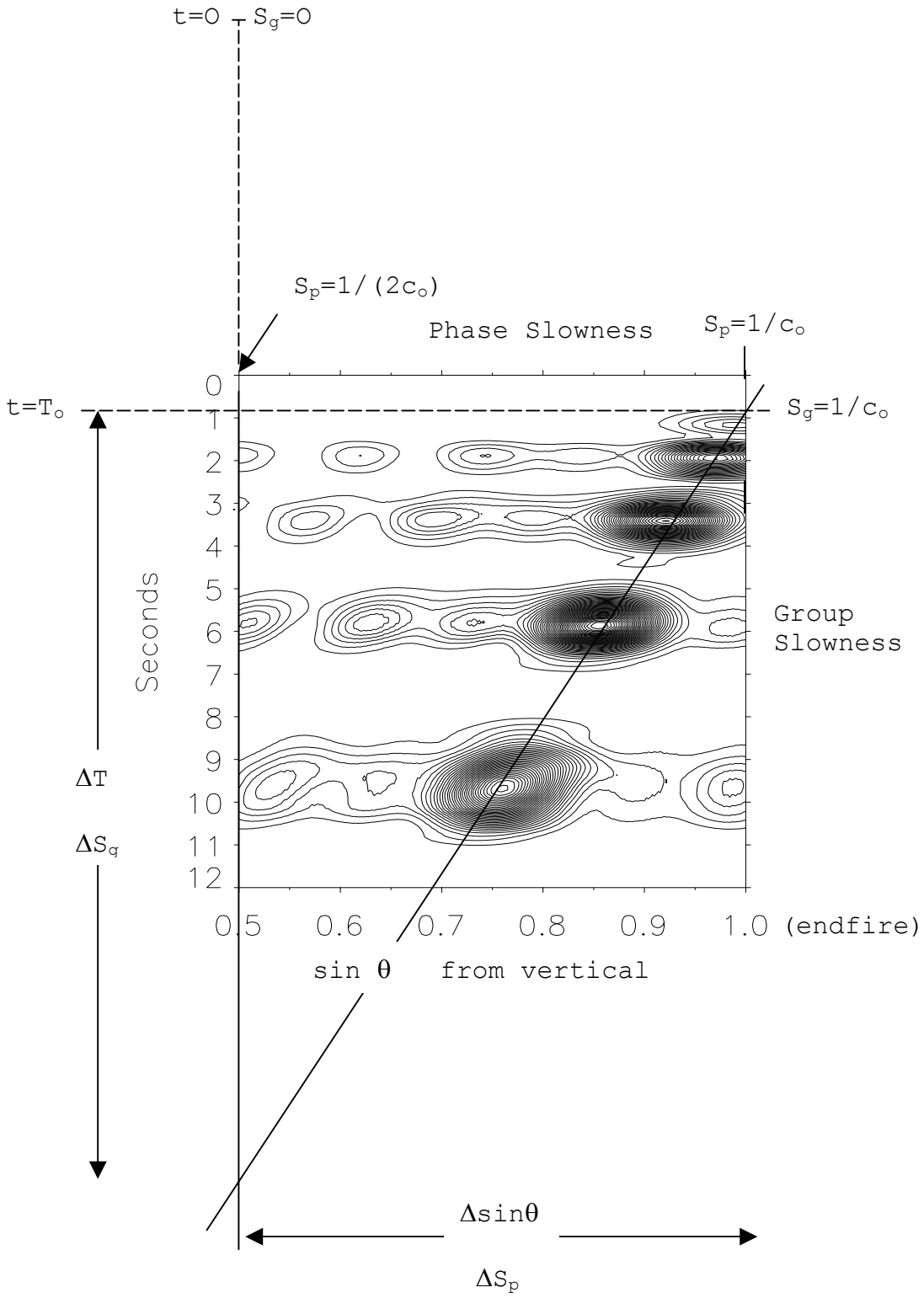

Figure 5.1 Beam versus time diagram as group versus phase slowness diagram for the Eastern 51 km shot at 16 Hz
t=0 = detonation time T_0 *= first possible arrival*
S_g *= group slowness* S_p *= phase slowness*
θ *= angle of incidence*

Measurement of slope. The slope of the straight-line pattern is

$$slope = \frac{\Delta T}{\Delta \sin\theta} \tag{5.5}$$

It can be determined "automatically" and fast by using a standard straight-line fitting procedure. Because of the inevitable sidelobes (can be seen in Figure 5.1) and possibly noise bursts, the fitting is preceded by some masking and threshold setting. Maxima below a certain sin θ are also left out. β is found by

$$\beta_{meas} = -\frac{\Delta S_p}{\Delta S_g} = -T_0 \frac{\Delta \sin\theta}{\Delta T} = -\frac{T_0}{slope} \tag{5.6}$$

Here it is understood that the slope must be taken as negative. Thus it is not necessary actually to pinpoint pairs of modes, say identify them, in order to find β as Equation (4.1) might indicate, but only draw the line and find the slope.

The β values according to Equation (5.6) will now be compared to theoretical β values following Equation (4.3) and assuming β = 1 close to the receiver. Theoretical β values will be found for both bottom versus range and bedrock versus range profiles. For the E run outside 70 km the sediment thickness was set to 15 m.

5.2 The median of slope values

The line-fitting method can fail, however, due to fluctuations and irregularities in the data. In order to cut out (most of) way-off β values automatically, slope values for a group of close frequencies were first found. For instance, within a 1/3 octave band were computed 7 slope values from each of 1/12 octave filters with 1/24 octave spacing. Within a full octave band were computed 23 values etc. Then the final slope value was taken as the median of this group.

When the shots are relatively close to the receiver, the method becomes somewhat unstable and erratic, because the modes are not well resolved. Therefore shots inside 10 km have not been included in the study.

5.3 β as function of frequency for two sample shots

Figure 5.2 shows measured β values, for the two sample shots, taken over frequencies in 1/12 octave bands with 1/24 octave separation. Within roughly 10 - 100 Hz the values of β are reasonably stable, but with a slowly increasing trend in β. The W run has β values around 0.8 while the E run has β values around 1.0. There is higher variability towards both the low and the high frequency ends. A reasonable "area of interest" would therefore be the band just indicated, but establishing the limits will be done later. As will be shown, the over-all bandwidth within which the median method is applied has importance for the stability of the estimates.

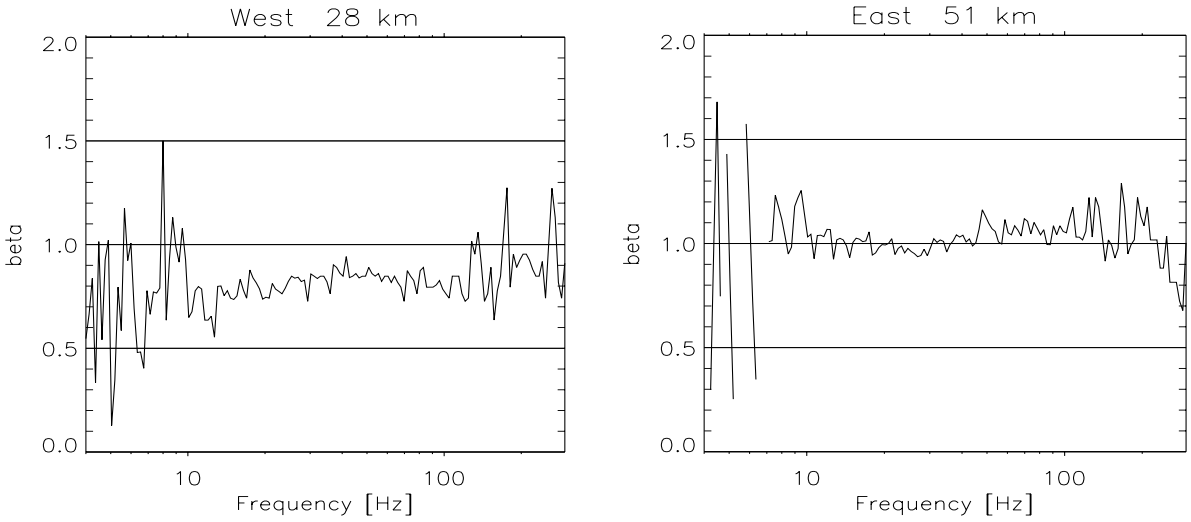

Figure 5.2 Measured β as function of frequency for the two sample shots
Basic filter bandwidth is 1/12 octave

5.4 Octave bands: measured versus theoretical β values for all shots

Measured β values were found for octave bands by the median method, with 23 of 1/12 octave filters within the band. Theoretical and measured β values will now be compared.

Figure 5.3 shows the W run for octave bands at 20, 40 and 80 Hz. Theoretical β profiles according to Equation (4.3) for water depth and top bedrock are shown as lines. They are in this run close together. The measured β values given as asterisks show good concentration, with little preference for any particular of the theoretical lines. There is not much difference between frequencies, but 40 Hz has the best concentration. The measured values have on average a slight tendency of being higher than the theoretical values.

Figure 5.4 shows the E run at 20, 40 and 80 Hz. The theoretical β values are to a large degree dominated by the depth depression at 12 - 20 km, the bedrock β values less so than those for the bottom. Now there is more difference between frequencies. At 20 and 40 Hz the measured values lie closest to the bedrock pattern, but a constant $\beta = 1$ would be a better assumption. At 20 Hz the depression appears to have no influence whatsoever. At 80 Hz the measured values lie closest to the bottom-related pattern. The depression has an influence, but not to the full extent of the theoretical line.

The range estimates will be treated in the next chapter. But to give a hint: the relative deviation of the measured β values from the theoretical ones will reflect the relative error in the range estimates.

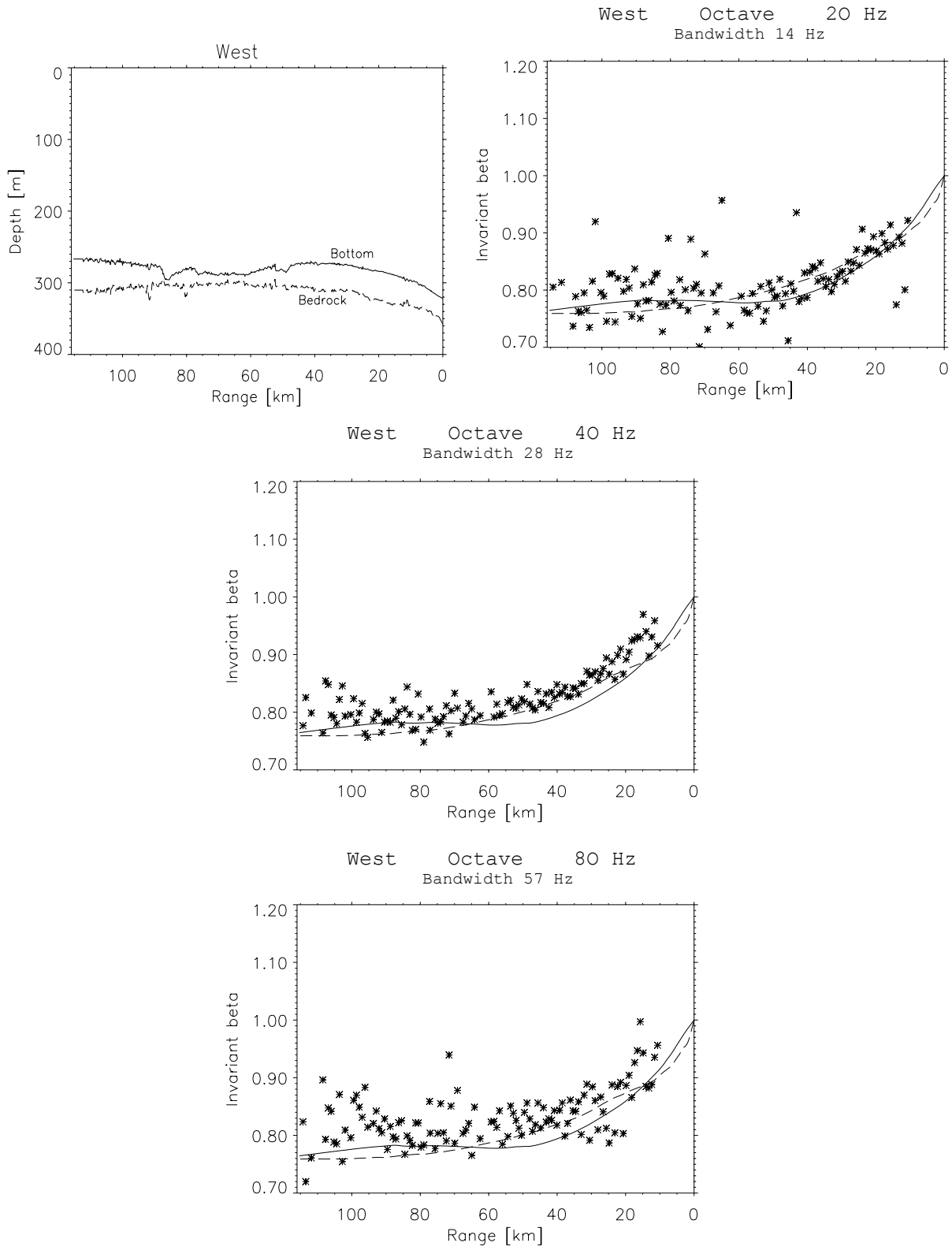

Figure 5.3 Measured and theoretical β values at different frequencies for the W run 1/1 octave bands

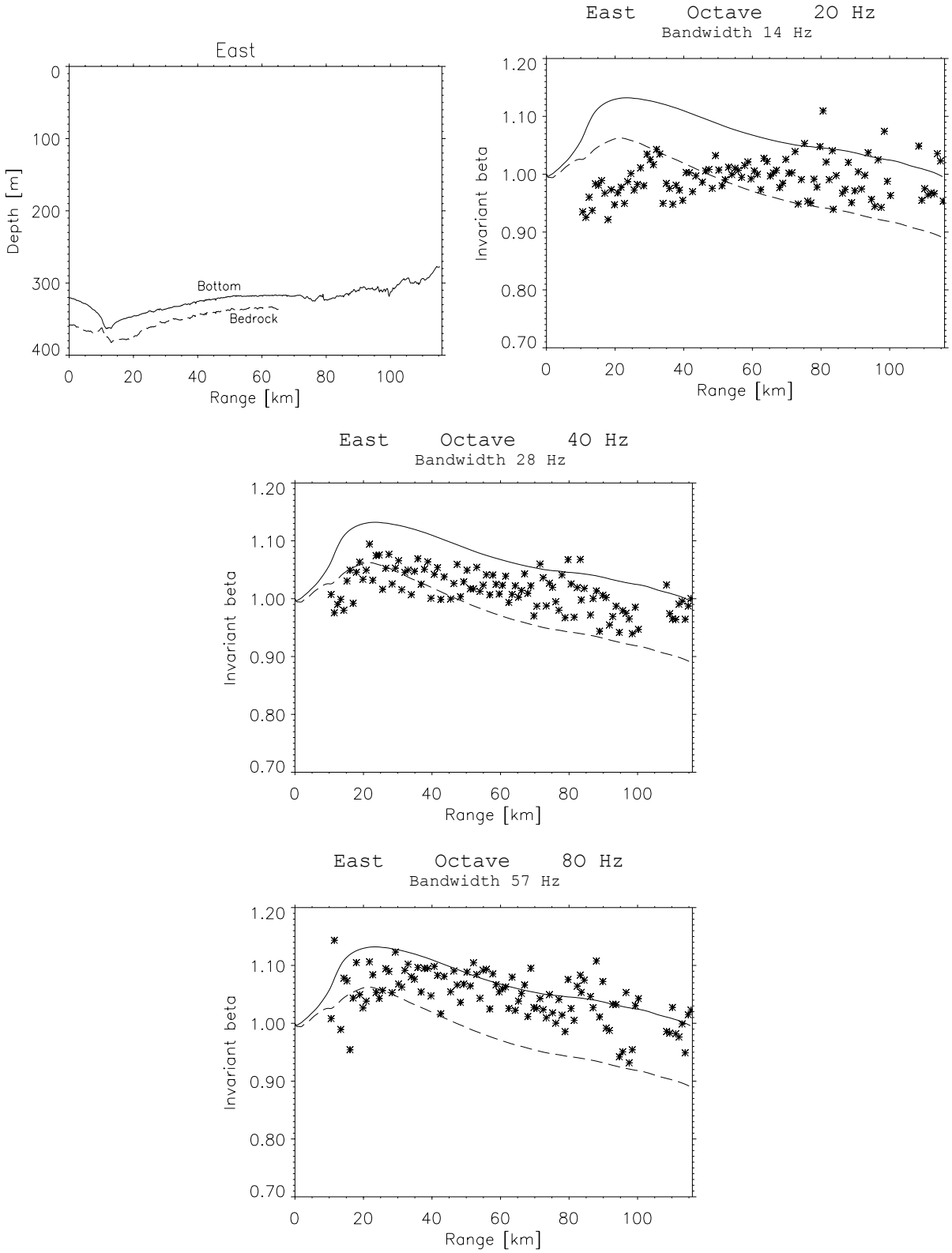

Figure 5.4 Measured and theoretical β values at different frequencies for the E run 1/1 octave bands

5.5 Smoothing the profiles

Compared to the W run, the fit for the E run was less satisfactory, although roughly within ±10%. The difference seemed to be somehow connected with the depression at 12 – 20 km. In order to investigate this, β lines from bottom and top bedrock profiles with much of the depression "filled in" were produced, Figure 5.5. Compared to Figure 5.3 there is a slightly better fit, but there still is a discrepancy. This will be discussed later.

5.6 The importance of bandwidth

There are two bandwidths to consider: the basic (narrow) filter bandwidth and the bandwidth over which the median is extracted. The basic filter bandwidth of 1/12 octave was chosen as a resolution compromise. Too narrow filters gave long impulse responses and bad time resolution. Too broad filters gave also bad time resolution because of high dispersion within the band and in addition bad angular resolution. Broader filters up to maximum over-all bandwidth were attempted, but gave inferior performance, even for close shots.

The over-all bandwidth has influence upon the stability of the β estimates. The greater the bandwidth, the better is the concentration or stability of β (and the range estimates to be shown later). Figure 5.6 shows results for the E run at 40 Hz when using 1/12, 1/3 and double octave bands, respectively. 1/1 octave band is already shown in Figure 5.4. The improvement in stability by going to larger bandwidths is evident.

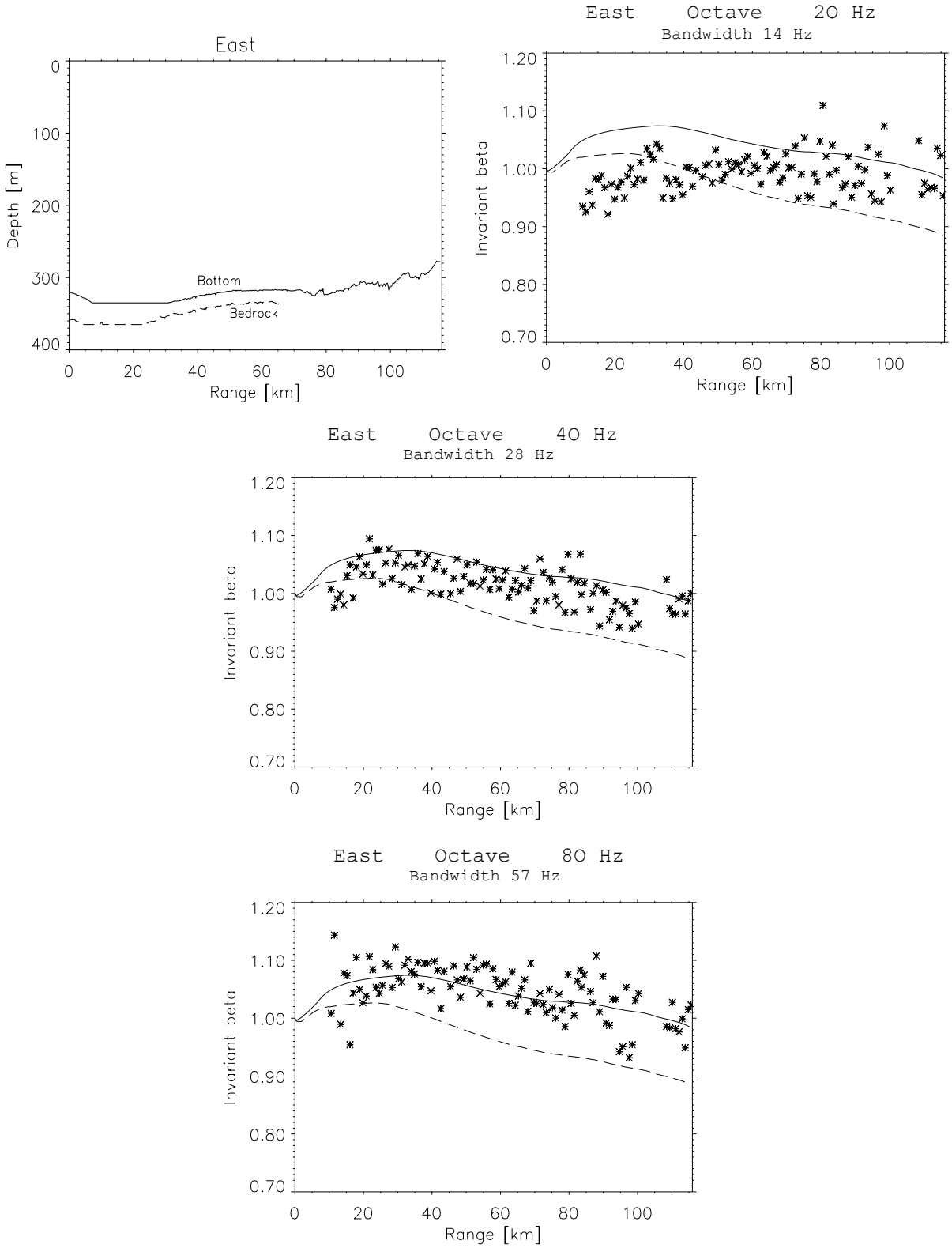

Figure 5.5 Influence of smoothing the depression
Measured and theoretical β values at different frequencies
1/1 octave bands

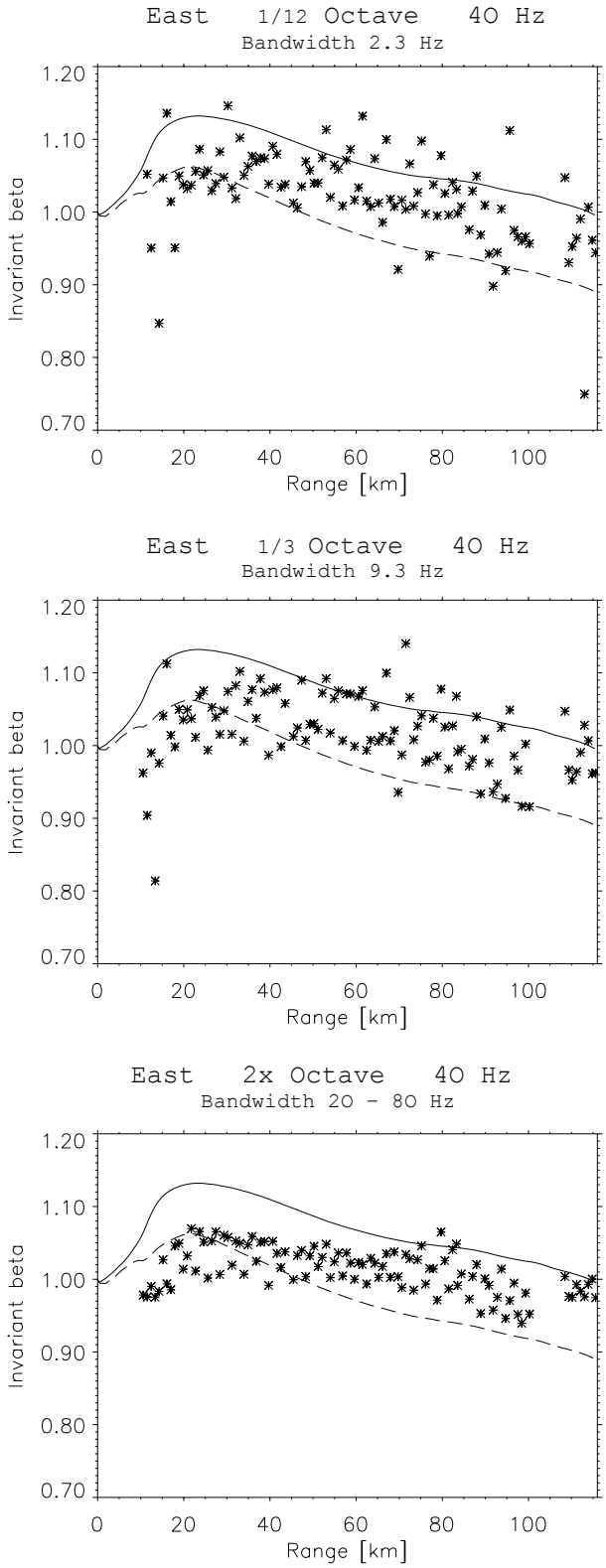

Figure 5.6 Measured and theoretical β values at different bandwidths for the E run 40 Hz center frequency

6 RANGE ESTIMATES

Range estimates will now be found. It will be assumed that Equation (1.4) applies, such that

$$R = -\beta_{theor} \frac{\Delta T}{\Delta S_p} = -\beta_{theor}\, c_0 \frac{\Delta T}{\Delta \sin\theta} = -\beta_{theor}\, c_0\ slope \tag{6.1}$$

The only actual measurement involved is estimation of the slope $\Delta T/\Delta \sin\theta$ of patterns in diagrams such as Figure 3.2. It will be assumed that the sound speed at the receiver c_0 is roughly known (an error of a few m/sec will do little harm). The arrival time T_0 does not enter. Theoretical β values were (as above) found from the bottom profiles and top bedrock profiles by Equation (4.3). It should be noted that Equation (6.1) actually has to be "solved" for R, because β_{theor} is a function of R. This is simply done by stepping R until equality is obtained.

Figures 6.1 – 6.2 give estimated shot ranges for the same cases as in Figures 5.3 - 5.4, presented in two different ways, one giving absolute range and the other percentage deviation. Theoretical top bedrock β values were used at 20 and 40 Hz, bottom β values at 80 Hz. The W run in Figure 6.1 has no special trends, but gives slightly underestimated ranges at 40 and 80 Hz. Using bottom β values at 40 Hz gave more underestimation (not shown). The spread is about the same for all ranges. The E run in Figure 6.2 at all frequencies gave as a trend some overestimation for the closer shots, and gave some underestimation for the longer at 20 and 40 Hz. The spread is about the same for all ranges, except for some extreme values at close ranges for 80 Hz.

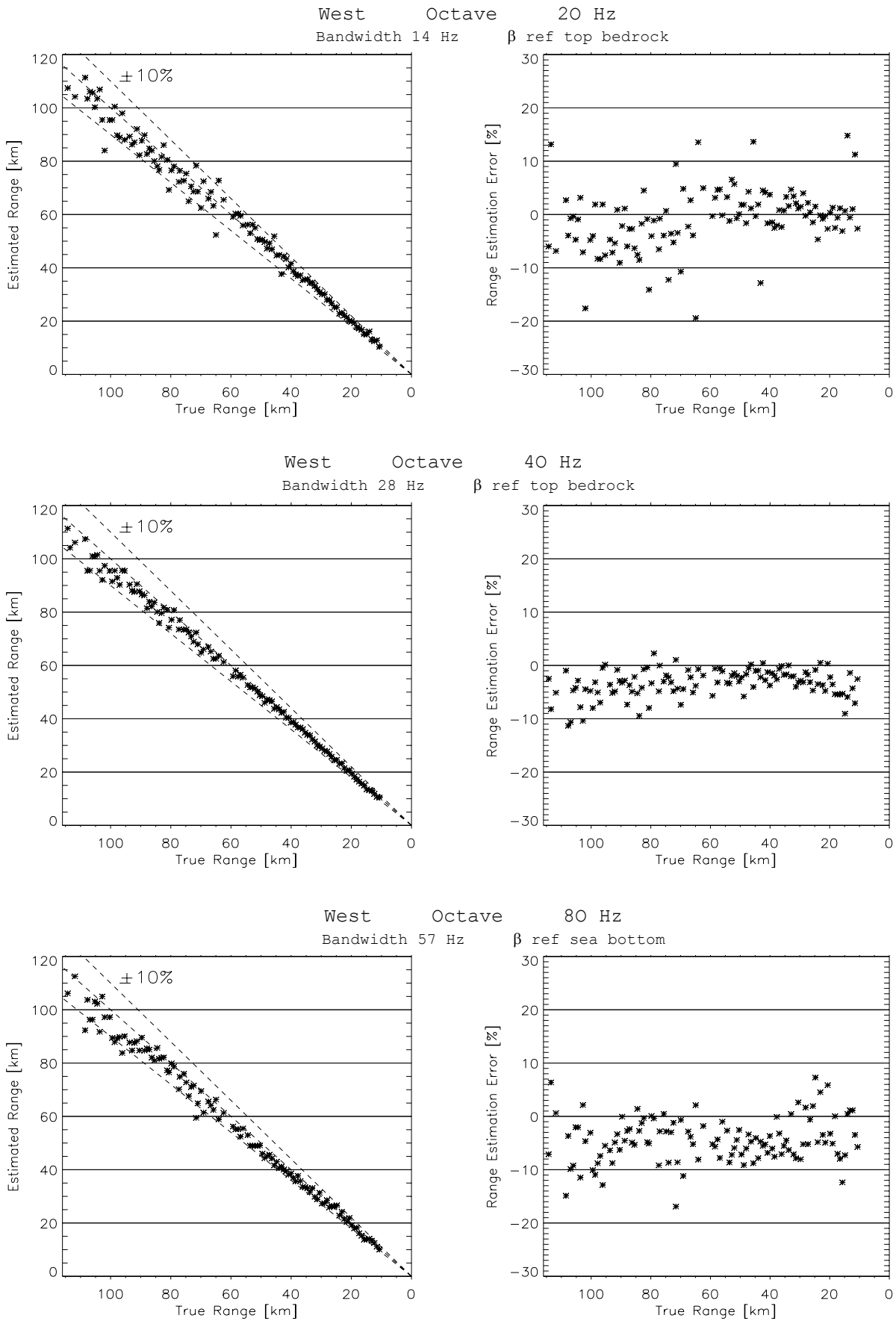

Figure 6.1 Range estimates in octave bands at different frequencies for the W run
20 and 40 Hz: β_{theor} from top bedrock 80 Hz: β_{theor} from sea bottom profile

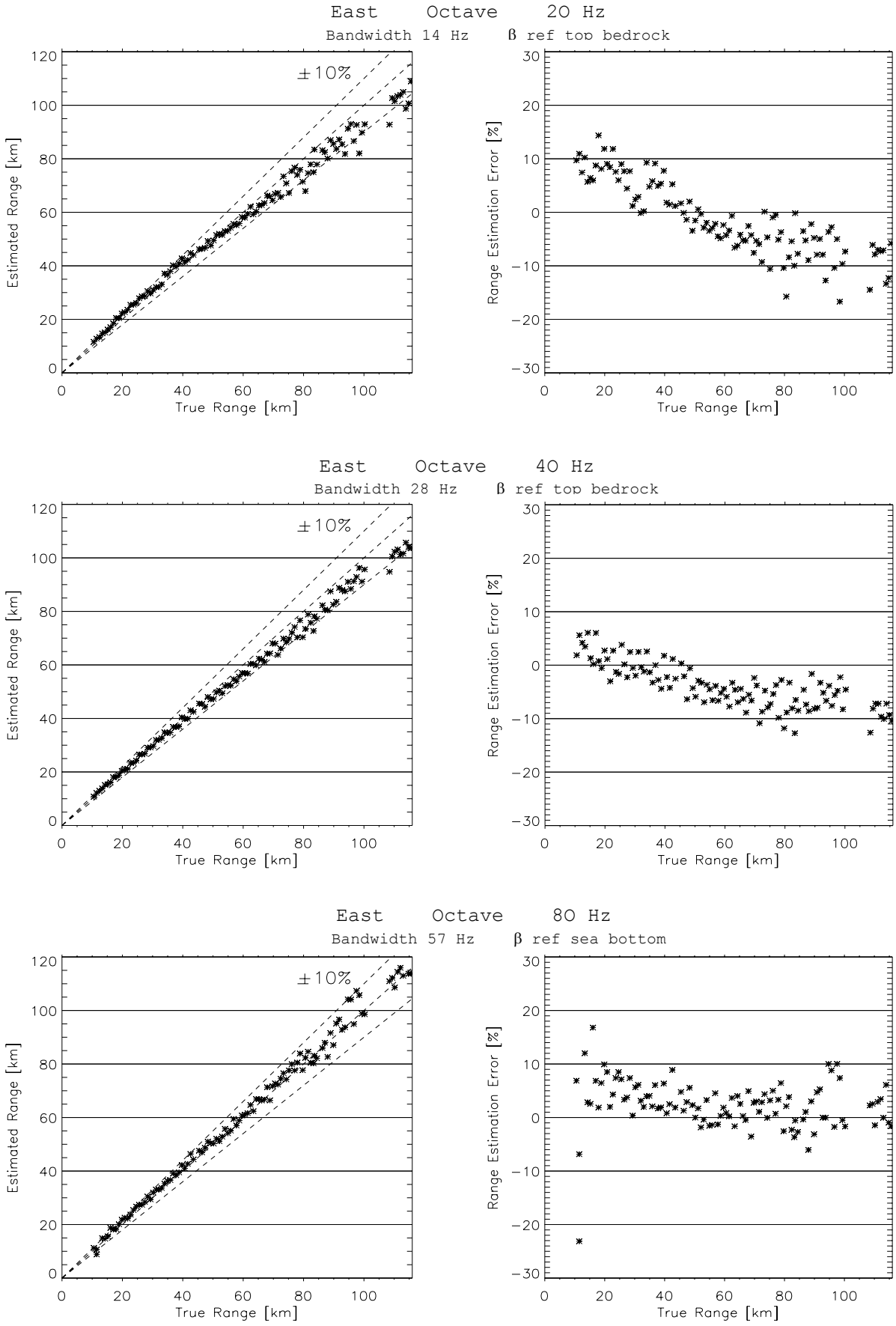

Figure 6.2 Range estimates in octave bands at different frequencies for the E run
20 and 40 Hz: β_{theor} from top bedrock 80 Hz: β_{theor} from sea bottom profile

6.1 Smoothing the profiles

‘Filling-in” the depression at 12 – 20 km as shown in Figure 5.5 gave slightly better results (not shown) than those in Figure 6.2.

6.2 Ignoring the changing bathymetry

Figure 6.3 shows the E run with the theoretical invariant set to $\beta = 1$ for all ranges, i e with no regard for the bottom or bedrock profiles. This gives at 20 and 40 Hz better estimates than those in Figure 6.2.

6.3 Variation of over-all bandwidth

Over-all bandwidth plays an important role. Figure 6.4 shows the same cases as Figure 5.6. Here only diagrams for percentage deviation are given. The importance of bandwidth is evident. However, it may be of some interest that even narrow bands (1/12 octave) can give range estimates of some concentration (here roughly ±10%).

6.4 Pushing the frequency limits

In an attempt to stretch the frequency range, estimates below 20 Hz and above 80 Hz were made. The following gives about the limits for usable β concentrations and range estimates. Figure 6.5 (top) shows an octave around 16 Hz for the W run. The octave extends down to 11 Hz. Figure 6.5 (bottom) shows an octave at 160 Hz. The octave extends upwards to 225 Hz. Both octaves give estimates within ±20%. Figure 6.6 gives similar diagrams for the E run, with comparable concentrations.

6.5 “Best results”

Using the double octave around 40 Hz, i e 20 – 80 Hz, Figure 6.7 gives the best results obtained for range estimation, with both good concentration and good averages. For the W run, the bedrock β profile was used. For the E run $\beta = 1$ was chosen.

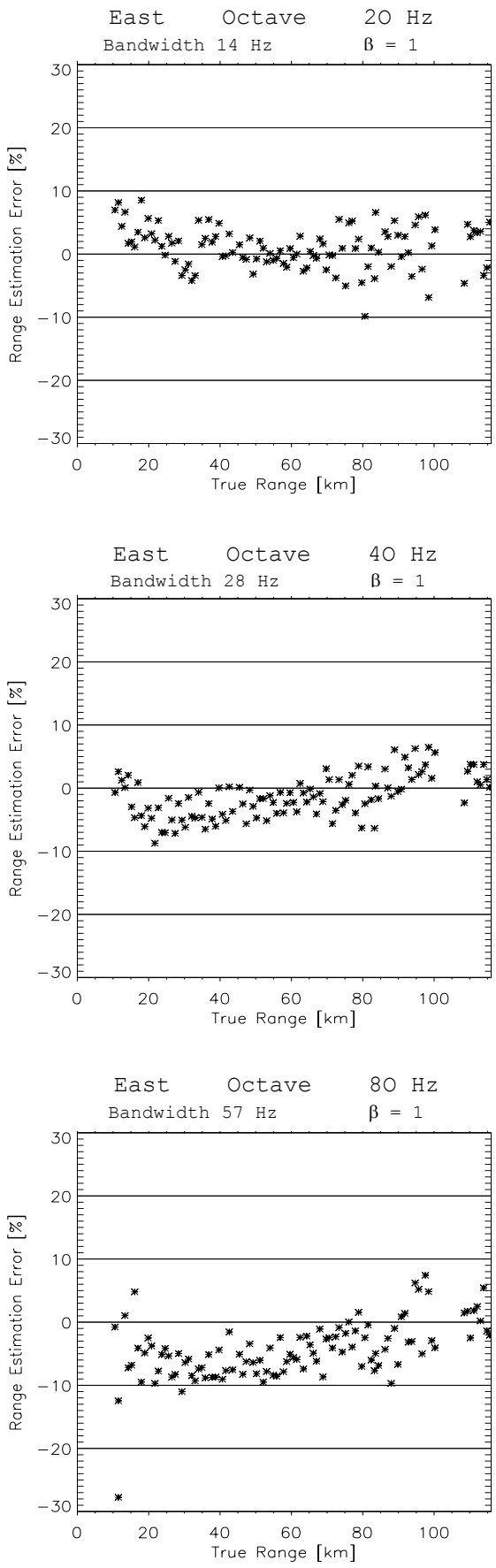

Figure 6.3 Range estimates in octave bands at different frequencies for the E run $\beta_{theor} = 1.0$

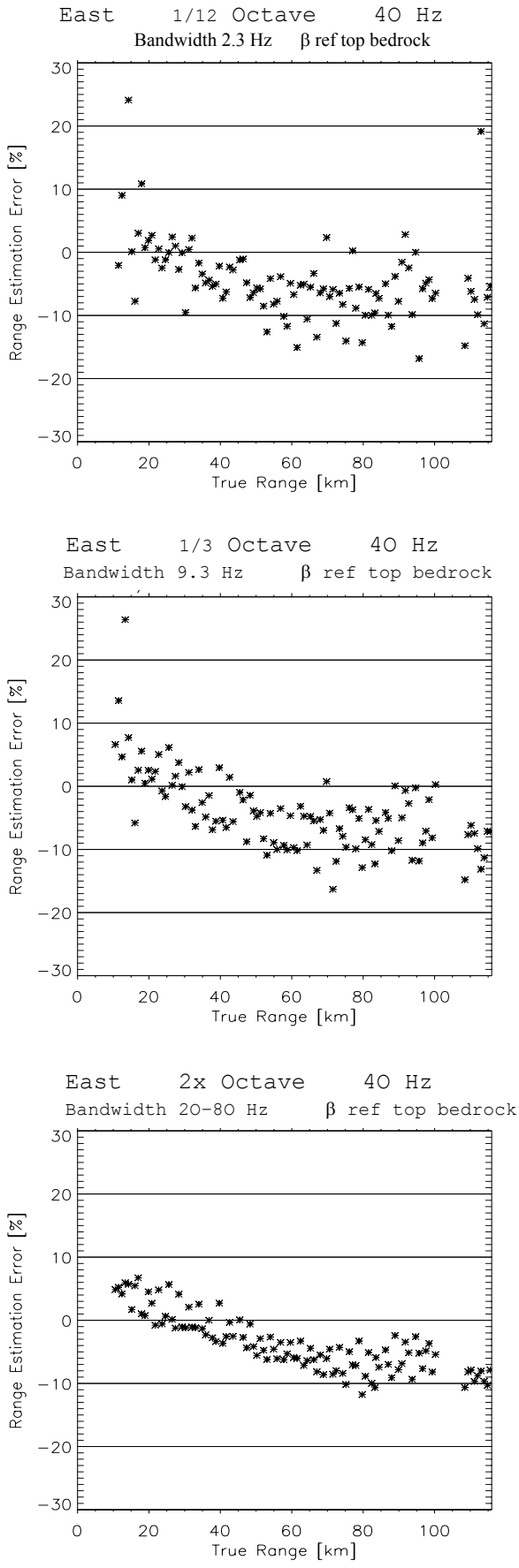

Figure 6.4 Range estimates in different bandwidths for the E run 40 Hz center frequency β_{theor} from top bedrock profile

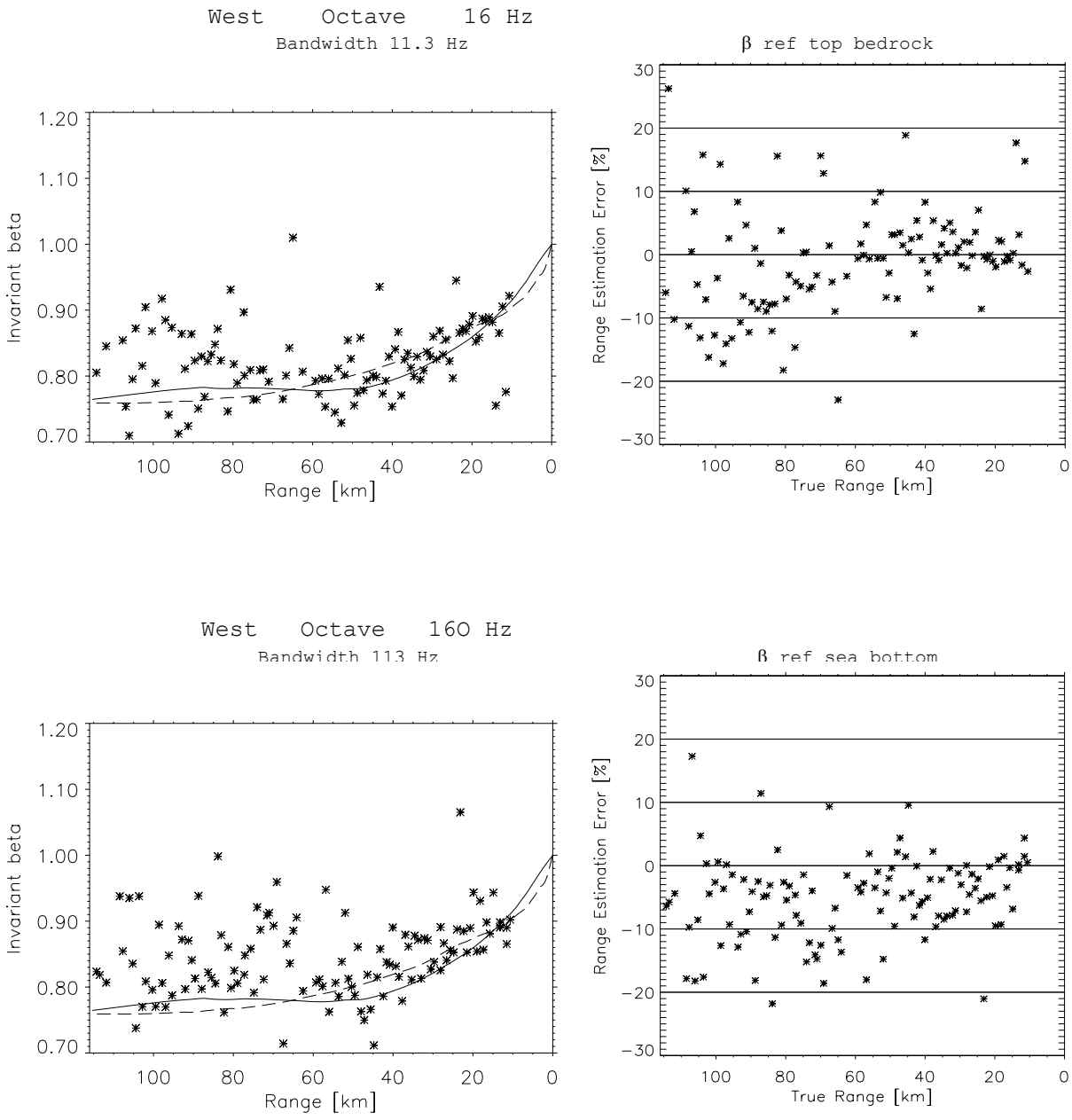

Figure 6.5 Pushing the frequency limits: 16 and 160 Hz for the W run
Octave bands
16 Hz: β_{theor} from top bedrock 160 Hz: β_{theor} from sea bottom profile

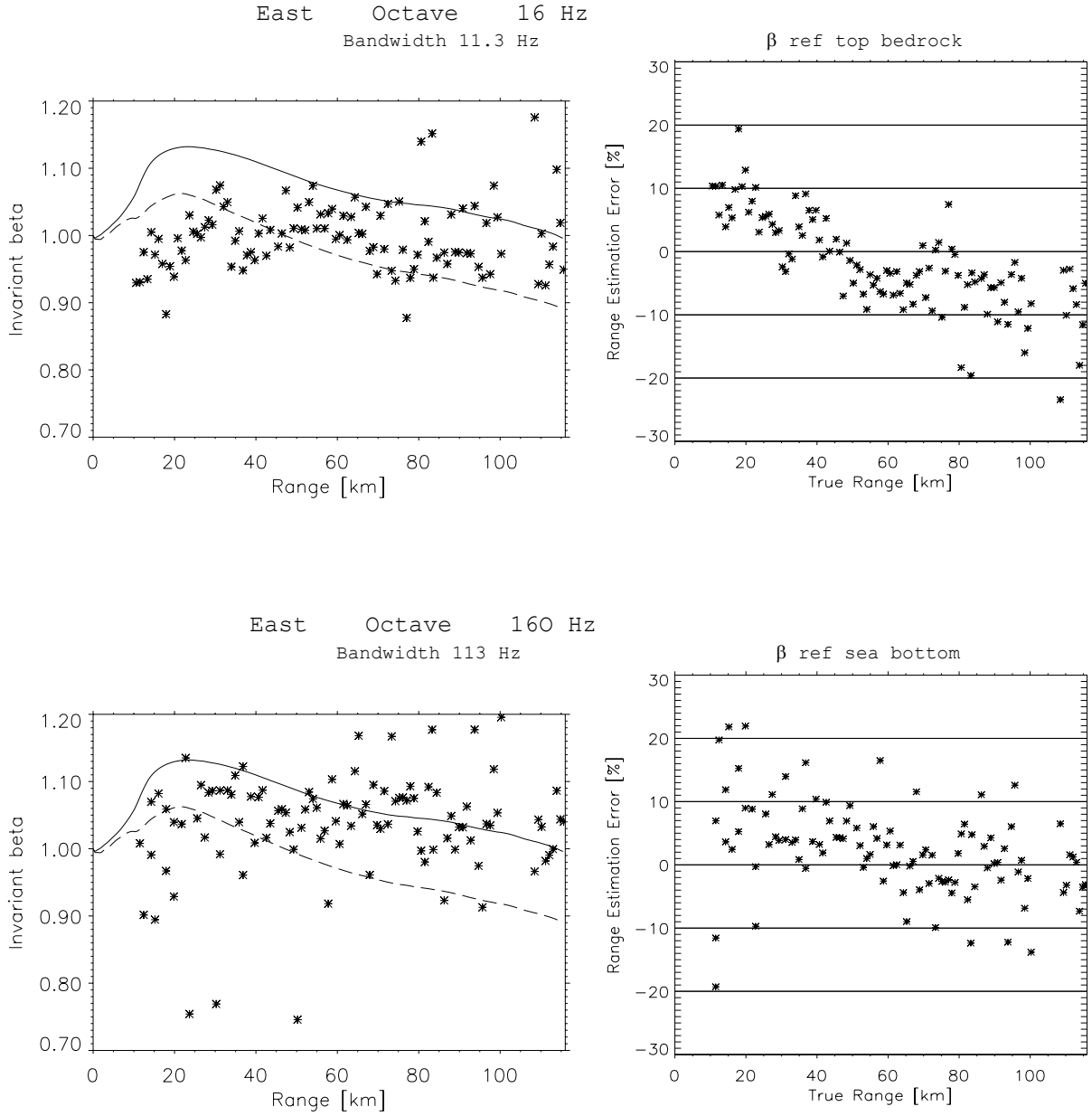

Figure 6.6 Pushing the frequency limits: 16 and 160 Hz the E run
Octave bands
16 Hz: β_{theor} from top bedrock 160 Hz: β_{theor} from sea bottom profile

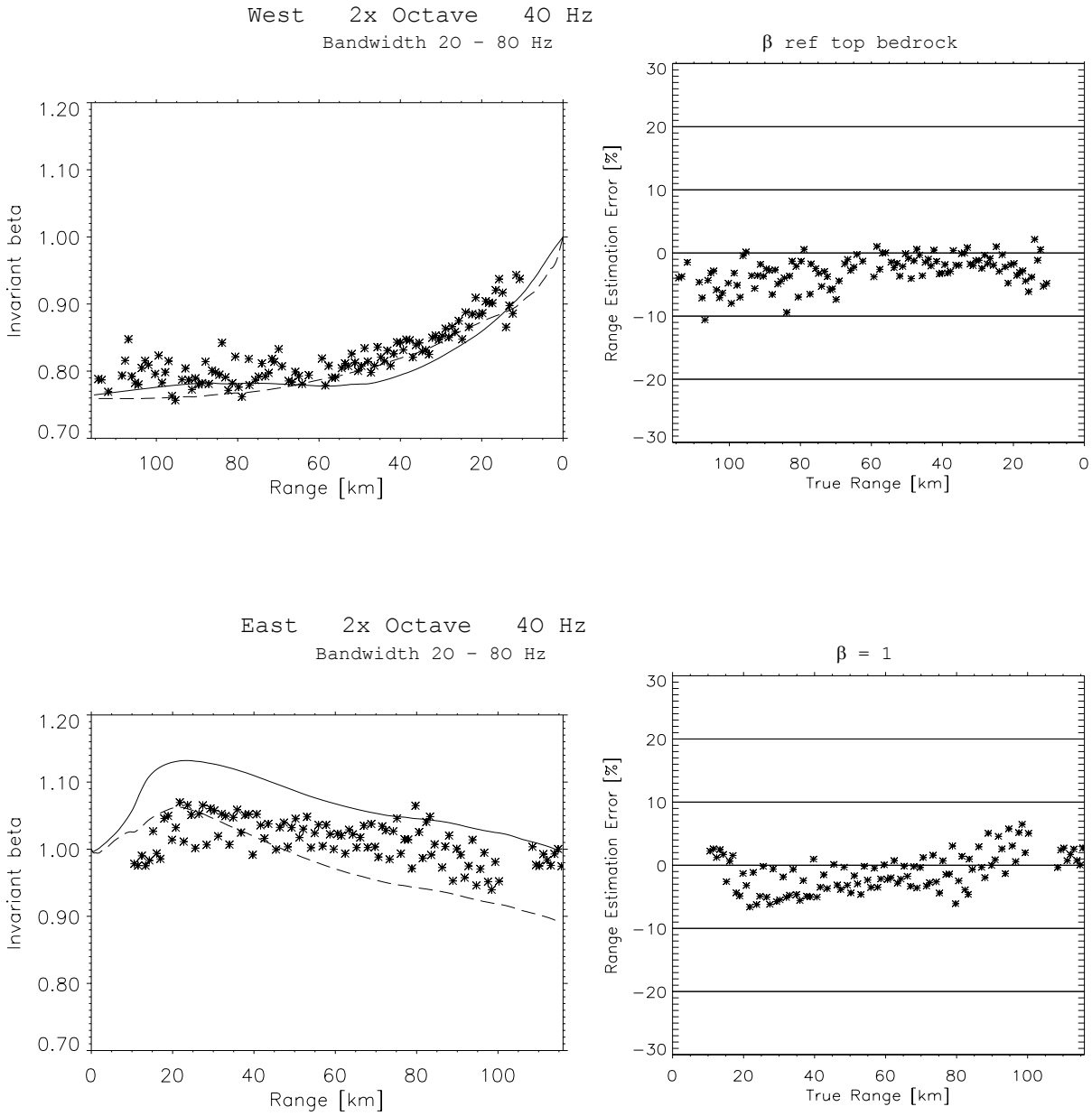

Figure 6.7 "Best results". Double octave bandwidth (20 – 80 Hz)
West: β_{theor} from bedrock profile East: β_{theor} = 1.0

6.6 The Eastern discrepancy

Contrary to the good agreement between theory and experiment in the Western run, the Eastern run showed some – although modest – differences at low frequencies, as demonstrated above. One could suspect that the water depth is changing too fast with range, so some ideal assumptions in connection with Equations (4.2) – (4.3) might be violated. On the other hand, in the W run the water depth changes relatively fast with range too, and that gives no problem. But there might be part(s) of the E run when the measured bottom or bedrock profiles miss the true steepness. There might also be some unknown features in the bottom compositions.

There is a main difference between the Western and Eastern runs. In the Western run there is a smooth and uniform change of slope in the vicinity of the receiver. The propagation is over more or less flat areas with downslope near the receiver. In the Eastern run there are more dramatic changes inside 20 km. The propagation is first downslope, then upslope. The Eastern run also has in its deeper parts a cold layer close to the bottom, as Figure 2.4 indicates. Closer investigation of the approximations, and maybe modelling based upon more fine-grained geophysical inputs could give an explanation for this, and provide better β profiles.

For the Eastern run, with its relatively large irregularities in the vicinity of the receiver, it was best at low frequencies to assume that $\beta \approx 1$, as bottom or bedrock β profiles made things worse. In the present case, this reduced the estimation errors by a half. For both runs there is a tendency, although not strong, for the measured β values on average to lie closer to $\beta = 1$ than what the present theory with its somewhat idealized assumptions predict.

7 CONCLUSIONS

Group speeds are difficult to measure locally. Phase speeds can be measured by means of an endfire array, and range estimates for shots can be found provided the so-called waveguide invariant β is known. For short ranges it was found by a Pekeris analogy that $\beta \approx 1$ for grazing angles less than 30°. For longer ranges and changing sea depth, theoretical β profiles were found by well-known formulas.

Both ranges and travel times were monitored during the experiment in question. β values could therefore actually be measured and checked against theoretical values. Extracting β values from measurements required a certain amount of processing of the beamformed signals. The 20 – 80 Hz frequency range was found to be the safest, but with possibilities within the larger band of 10 – 200 Hz. The accuracy and stability of the measured β values increased with the bandwidth used. Still, estimates better than ±20% were obtained even by using 1/12 octave (= ±3%) bandwidth.

In general, range estimates will be influenced by the quality of the array. For the present study, the array had 10 hydrophones of uneven spacing over 820 m, with 20 m as the smallest spacing, in fact a rather sparse array. More hydrophones might improve the frequency limits and the stability.

The Western run obtained the best concentrations and good fit to the true values. It was possible in octave bands to give range estimates within ±5% of the correct value, based solely upon the bottom and top bedrock profiles and an approximate value of the water sound speed.

For the Eastern run at low frequencies (20 – 40 Hz) the measured β values did not fit the theoretical values that well. The discrepancy is at present unexplained. Still, the range estimates were even then typically within ±10% of the correct values. The estimates improved towards ±5% by setting the invariant $\beta = 1$. At higher frequencies (80 Hz) the fit was better

using the sea bottom β profile. Typically there was a slight overestimation with a spread of ±5%.

It is worth noting that the relative spread in the range estimates was roughly constant over the whole range 10 – 115 km, except for an occasional increase by the closer shots.

References

(1) Eidem E J, Bendiksen B, Helgesen H (1999): Project SWASI: Technical cruise report Phase S-V 1999, FFI/RAPPORT-99/04955, Exempt from public disclosure

(2) Johnsen J (1999): SWASI II – Cruise report, Phase S-V 1999, FFI/NOTAT-99/05715, Exempt from public disclosure

(3) Søstrand K A (2000): Nøyaktig måling av lydens gruppehastighet i en lang undervanns transmisjonskanal, FFI/NOTAT-2000/05073, Unntatt offentlighet

(4) Solberg C E (2001): Geoakustiske modeller for MFP eksperiment i Barentshavet august 1999, FFI/RAPPORT-2001/00335

(5) Chuprov S D (1982): Inteferentsionnaya struktura zvukovogo polya v sloistom okeane (Interference structure of a sound field in a layered ocean), in Akustika Okeana. Sovremennoe sostoyanie (Ocean Acoustics. Current state), ed by L M Brekhovskikh, I B Andreevoi, Nauka, Moscow 1982, pp 71-91 (In Russian)

(6) Brekovskikh L M, Lysanov Yu P (1991): Fundamentals of ocean acoustics, Springer-Verlag, New York, pp 140-145

(7) D'Spain G L, Kuperman, W A (1999): Application of waveguide invariants to analysis of spectrograms from shallow water environments that vary in range and azimuth, J Acoust Soc Am 106 (5), November 1999, pp 2454-2468

APPENDICES

A VERIFICATION OF GPS-BASED RANGES AND TRAVEL TIMES

A simple method for verification of correct GPS ranges and travel times is by checking the corresponding average sound speeds (= range/time). Figure A.1 shows this for the two runs. Average sound speed is about 1472 m/sec for shots close to the receiver. Eastwards it drops eventually to around 1469 m/sec, while westwards it increases to approx 1473 m/sec. All three source depths are included. Shallow charges are indicated by circles.

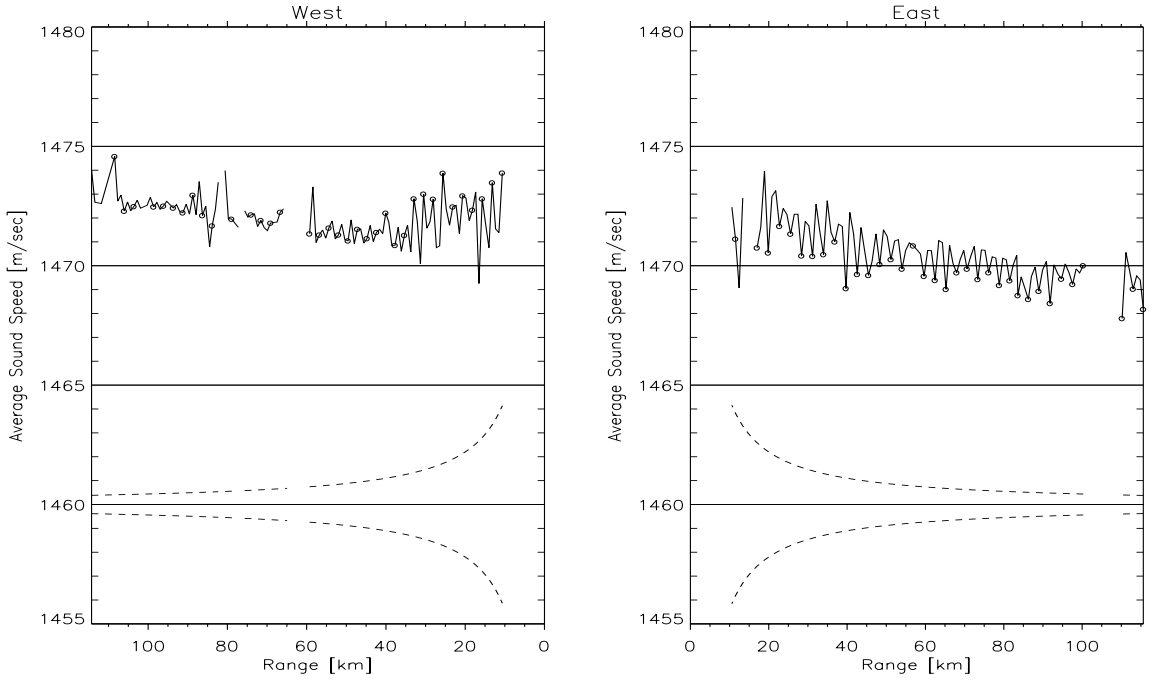

Figure A.1 GPS-based average sound speed values for the two runs
All three source depths. Circles: shallow (18 m) shots
Dotted lines: single depth theoretical spread according to (3)

In the E run the shallow charges show lower sound speeds than the deeper. This shallow/deep difference is almost constant with range. If this had something with the local geometry at the transmitting vessel to do, the difference should be smaller with increasing range. Not being the case, it is likely that the shallow/deep differences are right, and are due to the actual sound speed conditions.

In the W run shallow and deep charges give about the same speed for the longer ranges, and the opposite shallow/deep trend of Run E for the closer ranges. There is an unexplained change around 33 km. By the same argument as above, the values are probably right.

The original aim was to bring the range error down towards ±15 m and the travel time error towards ±10 msec (3). Translating these into speed error gives the expressions

$$c_0 = \frac{R}{T} \tag{A.1}$$

$$\Delta c_0 \approx \left|\frac{\partial c_0}{\partial R}\right| \Delta R + \left|\frac{\partial c_0}{\partial T}\right| \Delta T = \frac{c_0}{R}(\Delta R + c_0 \Delta T) \tag{A.2}$$

$$\pm \Delta c_0 = \pm \frac{44000}{R} \tag{A.3}$$

At the bottom of Figure A.1 these limits are indicated. In comparing them with the measured values, one should bear in mind that they only express variations around a mean value, which from West to East will go from 1473 m/sec to 1469 m/sec. For any of the three charge depths, the variations of actual speeds are comparable in magnitude to the theoretical errors.

B DISPERSIVE TRANSIENTS AND BEAMFORMING

What is to be demonstrated now can all be deduced from theory and simulation, and are well-known features of the acoustic waveguide. However, it is always gratifying to see the same happen with real signals.

Figure B.1 shows signals recorded at the ten hydrophones of the horizontal array for an Eastern shot at 37 km. Center frequency is 10 Hz, bandwidth is 1/6 octave, i e ± 0.6 Hz. Four modes can be seen as envelopes enclosing the frequency components in the band. There are also some small disturbances, such as that in front of Mode 4. Signal #31 is a little more than 0.5 sec later than signal #22. Still,

> Signal #31 is what signal #22 would look like after travelling 820 m along the array.

But they will not be exactly alike. What is not so readily seen in this picture is,

> As it moves horizontally, the signal will “stretch” in distance between the modes as higher mode numbers have lower group speeds, Figure 4.1. The mode envelopes themselves will also stretch.

By lining up the signals, i e give them the same starting point at Mode 1, Figure B.2 is produced. Here it can clearly be seen that signal #31 is longer than signal #22. The stretching of the blobs themselves is too small to be seen in this picture.

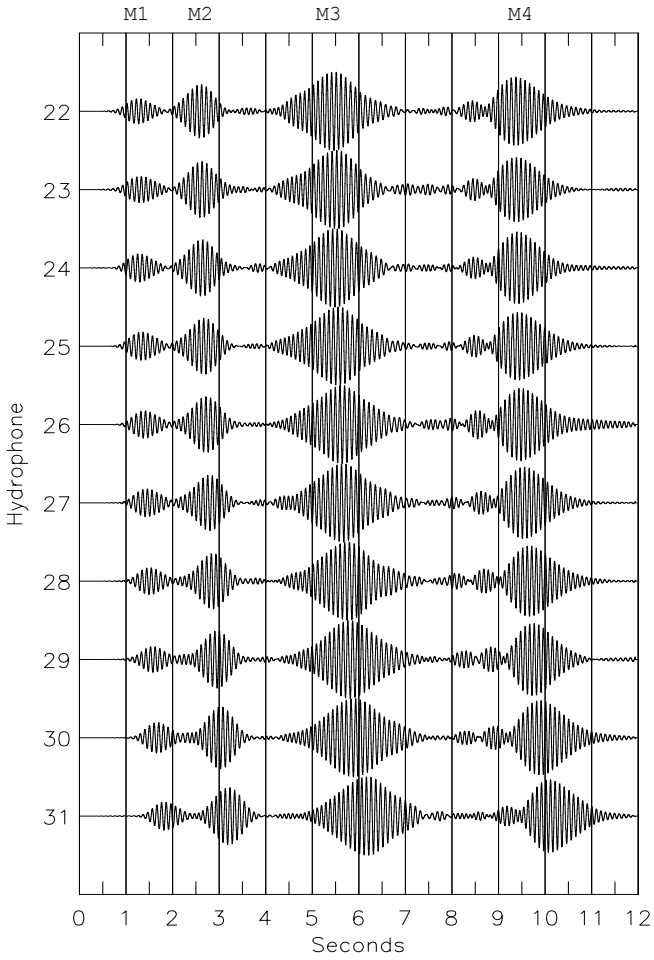

Figure B.1 All hydrophone signals for the Eastern 37 km shot at 10 Hz in 1/6 octave bands

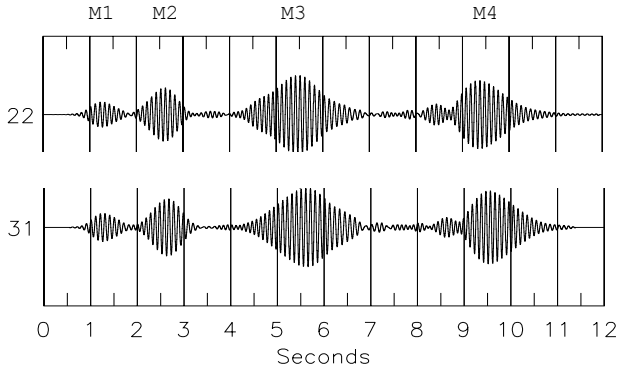

Figure B.2 Demonstration of signal stretching
Lined-up hydrophone signals for first and last hydrophone

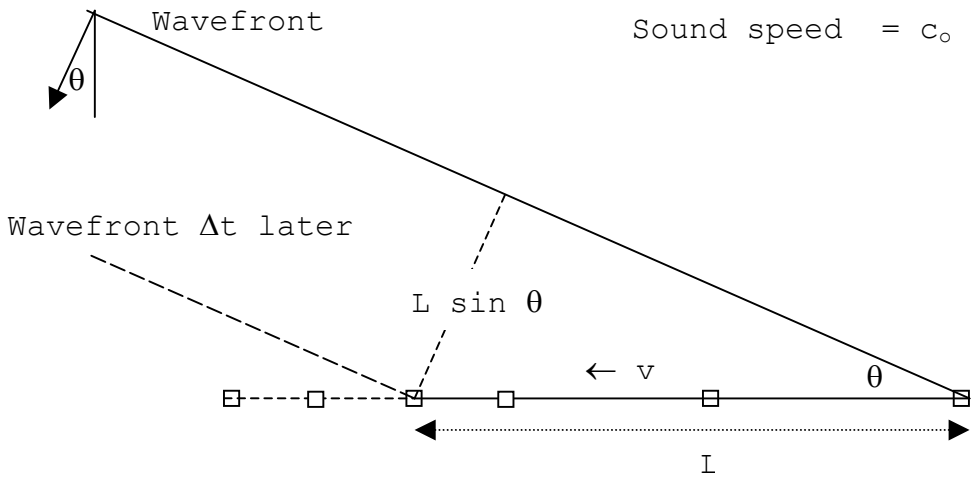

$$t = \frac{L\sin\theta}{c_0} \qquad v = \frac{L}{\Delta t} = \frac{c_0}{\sin\theta}$$

Figure B.3 The connections between angle of incidence, delay and phase speed

Phase speeds. Figure B.3 illustrates the correspondence between angle of incidence θ, delays and phase speed v. As a wavefront intersects the array, the zero crossings will move horizontally. Over length L the transit time will be

$$\Delta t = \frac{L\sin\theta}{c_0} \tag{B.1}$$

The speed of the zero crossings along the array will be

$$v = \frac{L}{\Delta t} = \frac{c_0}{\sin\theta} \tag{B.2}$$

The operation of a delay-and-sum beamformer is first to line up the hydrophone signals, then sum. Line-up amounts to compensate for the delays in the water according to the expression

$$Delay_i = \frac{L_i}{v} \tag{B.3}$$

Here L_i is distance along the array to a reference hydrophone i, and v is the signal speed *along* the array.

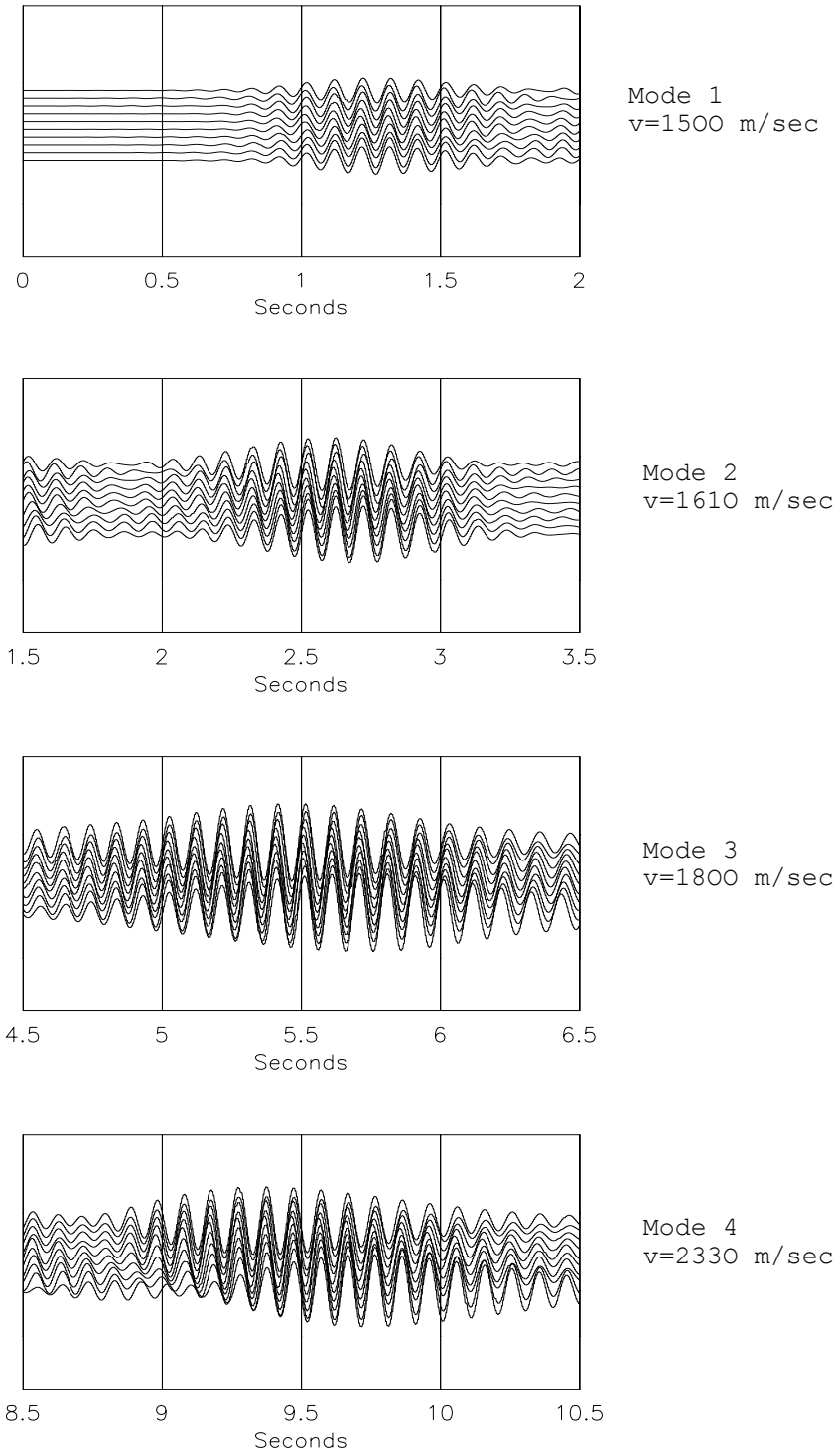

Figure B.4 Lined-up hydrophone signals for the different modes. Inserted delays = L_i/v

It will now be demonstrated that signals of individual modes must be lined up by using speeds v which can be far higher than the sound speed of 1470 m/sec. Take for instance the signal section from 8.5 – 10.5 sec around Mode 4. Delays are put in according to Equation (B.3). After some cut and try, v = 2330 m/sec is settled for. Figure B.4 (bottom) shows the result, where for illustration purposes the vertical spacing between the traces have been shrunk. The waveforms in Mode 4 have now been lined up properly. Summation would produce the

maximum beam outputs. This value of 2330 m/sec is *unique* since the array has uneven hydrophone spacing. No other value of v will give full line-up. Figures B.4 shows also similar diagrams for Modes 1, 2 and 3 at speeds v = 1500, 1610 and 1800 m/sec, respectively. All these speeds are *phase speeds*. Checking with Figure 4.1 will support this (the speeds compare very well). Thus

> A delay-and-sum beamformer can measure phase speeds.

Group speeds. Trying to line up the *envelopes* of Mode 4 gives Figure B.5. The necessary speed for this is v = 1100 m/sec. Lining-up of the other modes was more uncertain. Here v is the *group speed*. This is supported by Figure 4.1. But

> After envelope extraction a delay-and-sum beamformer can in principle measure group speeds. In practice long arrays are required, longer than the present one.

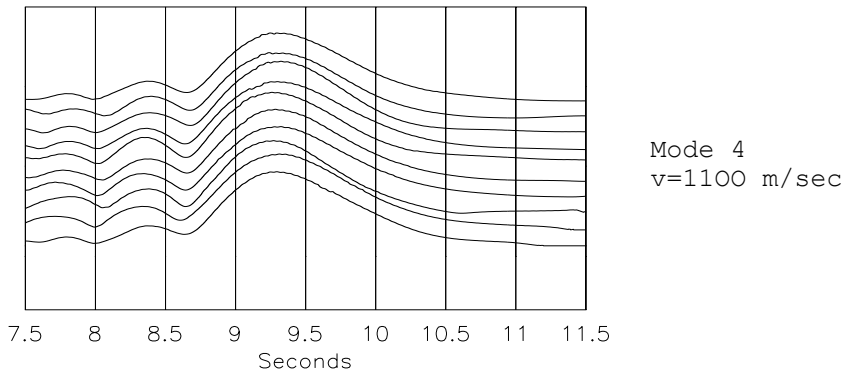

Figure B.5 Lined-up hydrophone signal envelopes for Mode 4

In Figure B.4 (bottom) it is possible to see that the envelopes of the first and the last hydrophones are shifted with respect to each other. In fact, this picture demonstrates both phase and group speeds. Piecing together the results above and drawing some conclusions,

> The envelopes will move with group speeds and the zero crossings will move with phase speeds. Thus the contents in each blob will move faster than the blob itself. As the signal moves in space, wave cycles will disappear at the front end of the blob, and new ones will appear at the back end. This means that, as it moves along and broadens, the envelope will contain an increasing number of signal cycles.

A feature distinguishable in Figure B.1 is,

> Because of the nonzero bandwidth of the signal, the highest frequencies will lie first in a blob. This is because higher frequencies have the largest group speeds (Figure 4.1). However, maybe a little puzzling, the zero crossings at the back end will move faster than those at the front end. This is because lower frequencies have higher phase speeds (Figure 4.1).

DISTRIBUTION LIST

FFIBM **Dato:** 10 December 2002

RAPPORTTYPE (KRYSS AV)	RAPPORT NR.	REFERANSE	RAPPORTENS DATO
X RAPP ☐ NOTAT ☐ RR	2002/04849	FFIBM/786/115	10 December 2002
RAPPORTENS BESKYTTELSESGRAD		ANTALL TRYKTE UTSTEDT	ANTALL SIDER
UNCLASSIFIED		35	43
RAPPORTENS TITTEL		FORFATTER(E)	
RANGE LOCALIZATION OF 10-100 KM SHOTS BY MEANS OF AN ENDFIRE ARRAY AND A WAVEGUIDE INVARIANT		SØSTRAND Knut A	
		FORDELING GODKJENT AV AVDELINGSSJEF:	
Jarl Johnsen		Jan Ivar Botnan	

EKSTERN FORDELING

ANTALL	EKS NR	TIL
1		FO/E
1		Ved: Asgeir Berg
1		Ved: Einar Lunde
1		FLO/SJØ
1		Ved: Svein Mjøsnes
1		NTNU: Ved Jens Hovem
		7034 Trondheim
1		Ross Chapman
		School of Earth and Ocean Sciences
		Univ of Victoria
		P O Box 3055
		Victoria, BC V8W 3P6, Canada
1		UVB.skvadron 1
1		Ved: Orl kapt Yngve Skoglund
1		Andøya flystasjon, 333 skvadron
1		Ved: Kaptein Steinar Bråthen
1		SACLANT Undersea Research Centre
		Viale San Bartolomeo 400
		I-19138 San Bartolomeo
		La Spezia, Italy

INTERN FORDELING

ANTALL	EKS NR	TIL
14		FFI-Bibl
1		FFI-ledelse
1		FFIE
1		FFISYS
1		FFIBM
1		FFIN
1		Forfattereksemplar (er)
2		Restopplag til Biblioteket
1		Avd ktr BM/Horten
		Elektronisk fordeling:
		FFI-veven
		Ellen J Eidem (EJE)
		Trond Jenserud (TJe)
		Jarl Johnsen (JKJ)
		Tor Knudsen (TKn)
		Torgeir Svolsbru (TSu)
		Connie E Solberg (CES)
		Tommy Torgersen (TTo)
		Dag Tollefsen (DTo)
		Elling Tveit (ETv)

FFI-K1 Retningslinjer for fordeling og forsendelse er gitt i Oraklet, Bind I, Bestemmelser om publikasjoner for Forsvarets forskningsinstitutt, pkt 2 og 5. Benytt ny side om nødvendig.